

Shear modulus of the hadron–quark mixed phase

Nathan K. Johnson-McDaniel^{1,2} and Benjamin J. Owen¹

¹*Institute for Gravitation and the Cosmos, Center for Particle and Gravitational Astrophysics,
Department of Physics, The Pennsylvania State University, University Park, PA 16802, USA*

²*Theoretisch-Physikalisches Institut, Friedrich-Schiller-Universität, Max-Wien-Platz 1, 07743 Jena, Germany*

(Dated: February 8, 2019)

Robust arguments predict that a hadron–quark mixed phase may exist in the cores of some “neutron” stars. Such a phase forms a crystalline lattice with a shear modulus higher than that of the crust due to the high density and charge separation, even allowing for the effects of charge screening. This may lead to strong continuous gravitational-wave emission from rapidly rotating neutron stars and gravitational-wave bursts associated with magnetar flares and pulsar glitches. We present the first detailed calculation of the shear modulus of the mixed phase. We describe the quark phase using the bag model plus first-order quantum chromodynamics corrections and the hadronic phase using relativistic mean-field models with parameters allowed by the most massive pulsar. Most of the calculation involves treating the “pasta phases” of the lattice via dimensional continuation, and we give a general method for computing dimensionally continued lattice sums including the Debye model of charge screening. We compute all the shear components of the elastic modulus tensor and angle average them to obtain the effective (scalar) shear modulus for the case where the mixed phase is a polycrystal. We include the contributions from changing the cell size, which are necessary for the stability of the lower-dimensional portions of the lattice. Stability also requires a minimum surface tension, generally tens of MeV fm^{-2} depending on the equation of state. We find that the shear modulus can be a few times $10^{33} \text{ erg cm}^{-3}$, two orders of magnitude higher than the first estimate, over a significant fraction of the maximum mass stable star for certain parameter choices.

PACS numbers: 97.60.Jd, 26.60.Dd, 62.20.de, 04.30.Db

I. INTRODUCTION

Asymptotic freedom implies that matter at asymptotically high densities consists of deconfined quarks, and these densities may overlap with the range found in neutron stars.¹ This was first noted by Collins and Perry [1], although before the discovery of asymptotic freedom less concrete suggestions were made by Itoh [2] and Bodmer [3], and the first astrophysically concrete treatment (realistic maximum mass, etc.) was given later by Witten [4]. More recent developments include the realization that any quark matter in neutron stars may be in a color superconducting state. The most well-known such state is the so-called color-flavor locked (CFL) superconducting state present at asymptotically high densities [5], but there are other color superconducting states that may be present at lower densities—see [6] for a general review. Quark matter could thus have a crystalline structure with a very high shear modulus [7], which became relevant to gravitational-wave searches several years ago [8, 9].

Even if none of these mechanisms applies and quark matter itself is fluid, there is a generic and robust argument that neutron-star cores are filled with a mixed phase of hadron and quark matter, which has a crystalline structure due to electrostatic and surface-tension effects. Some recent gravitational-wave searches [10, 11]

have reached sensitivities for which the first rough estimate of the shear modulus of this mixed phase [12]—which is smaller than the estimates for quark matter—is relevant. Therefore it is worth a more careful calculation to get a better idea of which gravitational-wave searches become relevant to this broader range of theoretical models. The justification for the existence of the mixed phase is as follows:

Glendenning [13, 14] (see also [15, 16] for reviews) argued that the phase transition from hadrons to quarks happens gradually, with a mixed phase existing over a wide range of pressures. A neutron star containing such a mixed phase is called a hybrid star. The argument for this possibility is very robust (provided that the phase transition is first order, as is generally expected), relying on the fact that charge can be locally separated between the two phases while maintaining global neutrality; this is energetically favored because it allows the hadron phase to reduce its isospin asymmetry without producing leptons. Observational constraints, even the discovery of a $1.97 \pm 0.04 M_{\odot}$ pulsar [17], do not rule out the possibility that large regions of the most massive neutron stars are composed of the mixed phase: The input parameters of the models have more than enough uncertainty to allow high-mass stars [18–22]. (One can even still obtain pure quark cores in such massive stars, with appropriate parameter choices [20], though we do not consider such extreme cases here, for simplicity.)

Like the nuclear “pasta” phases in the crust (first discussed by Ravenhall, Pethick, and Wilson [23]), the hadron–quark mixed phase is thought to form a lat-

¹ We use the term “neutron star” to refer to any compact star made of cold-catalyzed matter, regardless of actual composition.

tice. This consists of charged blobs of the rare phase in a background of the common phase and has a varying dimensionality due to the competition between surface tension and the Coulomb force, as first suggested by Heiselberg, Pethick, and Staubo [24]. At the lowest pressure of the phase transition, small quark droplets form a 3-dimensional lattice in a background of hadrons. At higher pressures the droplets grow and give way to a 2-dimensional lattice of rods, then a 1-dimensional lattice of interleaved quark and hadron slabs. At even higher pressures the progression is reversed, with the quark slabs outgrowing the hadron slabs, then hadrons forming rods and droplets in a quark background before vanishing altogether.

These mixed-phase lattices can have a larger shear modulus than that of the crust, due mainly (in three dimensions) to the larger charge separation (from several hundreds to more than a thousand elementary charges per blob, rather than tens for nuclei). The shear modulus was first estimated very roughly by one of us [12], including a simple model of charge screening, the effects of which can change the result by orders of magnitude. A more detailed calculation was begun by Nayyar [25], and a rough estimate neglecting charge screening but including the surface energy is given in Sec. 7.7.2 of Haensel, Potekhin, and Yakovlev [26]. The latter also summarizes related work on other exotic phases: High shear moduli for pion condensates have been predicted as early as Ref. [27], and similar estimates were made even earlier for solid neutron cores which were proposed to explain glitches of the Vela pulsar [28].

Due to the high shear modulus of the mixed phase, hybrid stars could sustain much larger deformations than normal neutron stars. This has implications not only for pulsar glitches but also for gravitational-wave emission, both continuous and in bursts associated with magnetar flares [12]. Upper limits on the gravitational-wave energy emitted in magnetar flares have entered the range of theoretical predictions (up to 10^{49} erg for hybrid stars) [8, 11, 29, 30]. And the most interesting upper limits on continuous-wave emission, those that beat the indirect limits (see [31, 32] for reviews), are for several stars [9, 10, 33] within an order of magnitude of the 10^{-5} maximum ellipticity first estimated for hybrid stars [12] and at the level of the 10^{-4} maximum that applies if more recent results on the maximum crust breaking strain [34] hold for the mixed phase. Therefore, more detailed calculations of the crystalline structure of the mixed phase are interesting for the interpretation of gravitational-wave observations even now, and will become more so when the upgraded “advanced” detectors come on-line.

Here we improve upon previous estimates of the mixed-phase shear modulus [12, 25, 26] with the first detailed calculation. The implications for magnetar flares were discussed by Corsi and Owen [35]. We will present an improved calculation of the consequences for continuous waves elsewhere [36].

We use the standard models used by Glendenning [16]

for the hadronic and quark equations of state (EOSs), as well as the standard Gibbs method for calculating the bulk properties and lattice structure of the mixed phase. We thus use a relativistic mean field model for the hadronic matter. As Norsen and Reddy [37] note, this assumption can be of dubious validity for small regions of hadronic matter, since the fields do not take on their mean values in that case. However, this is not much of a concern for us, since, as Norsen and Reddy discuss, it is only a large effect for lower-dimensional hadronic blobs, and these are only present in stable stars for one of the EOSs we consider, where they have relatively large dimensions. (See Sec. II for further discussion.) We do not have to worry about such errors in our description of the quark blobs, since we are using an improved bag model for them. We also include the oft-neglected contribution from the surface tension to the pressure balance in a few of our EOSs, following [37–40].

We obtain significantly larger shear moduli than Ref. [12] primarily due to our inclusion of the contributions that arise from the change in the cell volume when one shears the lower-dimensional lattices. (Some of these contributions were considered by Pethick and Potekhin [41] for the case of the nuclear pasta in the crust. Additionally, the estimate of Haensel, Potekhin, and Yakovlev [26] is based on these contributions.) This is the most important improvement in our analysis. These contributions are necessary for the lower-dimensional lattices to be stable, and this stability leads to an EOS-parameter-dependent minimum surface tension. Additionally, for large but reasonable surface tensions, these contributions significantly increase the overall shear modulus of the lower-dimensional lattices.

Another fundamental improvement is that we treat the varying dimensionality of the pasta phases using dimensional continuation. This technique was first suggested by Ravenhall, Pethick, and Wilson [23] for the nuclear pasta in the crust, and then applied to the hadron–quark pasta by Glendenning [15]. It is a relatively simple way to approximate the complicated structure seen in, e.g., molecular dynamics simulations of nuclear pasta [42–45]. In order to perform the dimensionally continued lattice sums, we have developed a generalization of the standard Ewald method [46] (see [47] for a modern treatment). The Ewald method was used by Fuchs [48] in his pioneering calculation of elastic coefficients, and has very recently been used by Baiko [49] in a calculation of the effective shear modulus of the neutron star crust. The underlying dimensionally continued Poisson summation formula has been reported elsewhere by one of us [50]. Here we describe the practical implementation to the situation at hand, including the details of the “Ewald screening function” and the dimensional continuation of the specific family of lattices we consider.

We would have liked to dimensionally continue the family of root lattices, A_d^* , which solve the covering problem in dimensions $d \leq 5$ (see, e.g., Sec. 1.5 in Conway and Sloane [51]). However, as discussed in Sec. VB, there is

no obvious way of doing so. Instead, we split the lattice up into hyperlattices and introduce a freely specifiable interpolation function for the hyperlattices' separation. We find that our results are quite insensitive to the specific choice of this function (particularly given the much larger uncertainties in the input parameters).

In yet another improvement, we perform rather than guess the angle averaging to obtain a scalar shear modulus from the (anisotropic) elastic modulus tensor. This makes the assumption (standard in the literature) that there are many regions with random orientations, so that the mixed phase can be treated as a polycrystal. The magnetic fields present in a neutron star may cause this assumption to be violated, and relaxing it would be an interesting topic for further investigation.

We also use the full Debye (linear) model for charge screening rather than multiply the unscreened result by a simple correction factor. Even this is a simplified treatment of screening effects, particularly because it is linear. Also, because we treat the blobs as point charges, it means that we do not include the contribution of charge screening in our computation of the blobs' energy (which is used to obtain the blob size and lattice spacing). However a more detailed treatment (following, e.g., [37–40]) would be much more computationally intensive than the remainder of our approach, so we have left such investigations to future work. (Recent work by Endo [40] shows that the mixed phase can still occupy much of the star even with a nonlinear treatment of charge screening, though one cannot draw any definite conclusions about our results from Endo's because he uses different EOS parameters.) Some indication of the magnitude of the error we make in using the Debye model can be seen in the jumps in the shear modulus in the figures in Sec. VI.

We use electrostatic units and set $\hbar = c = 1$, so we will generally express masses in MeV and lengths in fm. All the computations were performed using MATHEMATICA 7's default methods to solve algebraic equations, numerically evaluate integrals, etc.

The paper is structured as follows: In Sec. II we review the models we use for the hadronic and quark EOSs, as well as how we compute the bulk properties, lattice structure, and charge screening of the mixed phase. In Sec. III, we give an overview of the elastic response of the lattice for the various integer dimensions, and show how we compute an average shear modulus in a dimensionally continued manner. We describe how to compute the relevant elastic constants in Sec. IV, and how to dimensionally continue the resulting lattice sums in Sec. V. We give our results for the shear modulus in Sec. VI, along with some discussion, and conclude in Sec. VII. We discuss various checks on our computations of the lattice sums in the Appendix.

II. MIXED PHASE

We model the hadronic and quark phases following Glendenning [16], using a relativistic mean field theory model for the hadronic matter (from Glendenning's Chap. 4), and an improved bag model description of the quark matter (from Glendenning's Chap. 8). (For simplicity, we do not consider the possibility of color superconductivity.) We have chosen to compute the EOSs “from scratch” instead of using any sort of tabulated EOS (except for the low-density EOS, which has a negligible effect on our results). This allows us to include the effects of surface tension on the EOS (as discussed in Sec. II C), and to investigate the effects of different EOS parameters on the shear modulus. It also lets us compute the Debye screening length, for which we need to know how the chemical potentials of the particle species vary with density. The models we use for the hadronic and quark phases are relatively simple, but should contain at least a rough description of the relevant physics for the situation under consideration. And given the significant uncertainties associated with any description of cold, dense matter, even relatively simple models should allow an adequate sampling of the relevant parameter space.

As mentioned previously—and emphasized by Norsen and Reddy [37]—the mean field theory description is not accurate for small regions of hadronic matter. However, this is of little concern for us, since this should only be a large effect for small, low-dimensional hadronic blobs, as discussed by Norsen and Reddy. The only EOS for which one obtains such blobs in stable stars, LKR1, has low-dimensional hadronic blob radii of ~ 10 fm, as illustrated in Sec. II C. Taking the hadron-kaon results from Norsen and Reddy to apply to our case, we see that the largest finite-size corrections will thus be $\sim 10\%$.

These EOSs depend on a variety of parameters, discussed in more detail in the following subsections. We consider a small collection of representative sets of parameters given in Table I. All of these parameter sets are chosen to yield a maximum Oppenheimer-Volkov (OV) mass compatible with the recent Demorest et al. [17] measurement of a $1.97 \pm 0.04 M_\odot$ neutron star.

Since the hadronic EOS we consider is only valid at densities well above neutron drip, we add on a standard low-density EOS for baryon number densities $n_B < 0.08 \text{ fm}^{-3}$. This is the combination of the Baym, Pethick, and Sutherland (BPS) [52] EOS for $n_B < 0.001 \text{ fm}^{-3}$ and the Negele and Vautherin [53] EOS for $0.001 \text{ fm}^{-3} < n_B < 0.08 \text{ fm}^{-3}$ used by Lattimer and Prakash [54]. We use the table provided by Kurkela *et al.* [55] at [56]. The precise choice of the low-density part of the EOS has a negligible effect on the maximum mass of a stable star.

Since we are interested in how large astrophysical effects could be, we generally choose our EOS parameters to be middle-ground estimates, but also consider some more extreme cases, to yield massive stars with a large region of mixed phase. (However, we do not consider stars with quark cores, for simplicity.) The Hy1 EOS is

taken from Nayyar [25], correcting an error in his code which led to a lower maximum mass. The Hy1' EOS changes the quark bag constant to obtain a larger region of mixed phase with more pasta phases in stable stars. The Hy1 μ and Hy1 σ EOSs each change the treatment of one portion of the calculation to give some indication of how much these affect our results: Hy1 μ uses a chemical-potential-dependent quantum chromodynamics (QCD) renormalization scale, while Hy1 σ includes the effects of surface tension on the pressure balance of the two phases; Hy1 $\mu\sigma$ includes both.

Following Weissenborn *et al.* [20], we also consider a case called LKR1 with the NL3 hadronic EOS parameters of Lalazissis, König, and Ring (LKR) [57]. These parameters give a very stiff hadronic EOS (a purely hadronic star would have a maximum mass of $2.78M_{\odot}$) and thus allow for neutron stars with a large region of mixed phase that still are compatible with a $1.97 \pm 0.04 M_{\odot}$ neutron star. For the corresponding quark EOS we picked parameters that lead to stable stars that include all the pasta phases. We also considered a case with somewhat generic parameters, generally picking them to be around the midpoint of the accepted range—this is the “generic” parameter set. These were not fine-tuned at all. Additionally, we have considered a variant that uses these more modern hadronic EOS parameters along with a bag constant and QCD coupling constant that yield a larger region of mixed phase—this is the generic' parameter set.

We plot these EOSs up to the maximum density present in a stable OV star in Fig. 1. We do not show the various flavors of the Hy1 EOS here, since the resulting traces are all very similar, though we do show the small violations of le Chatelier's principle for the Hy1 σ and Hy1 $\mu\sigma$ EOSs, compared with the Hy1 EOS in Fig. 2. (We do not show the trace for the Hy1 μ EOS, as it is almost identical to that for the Hy1 EOS.)

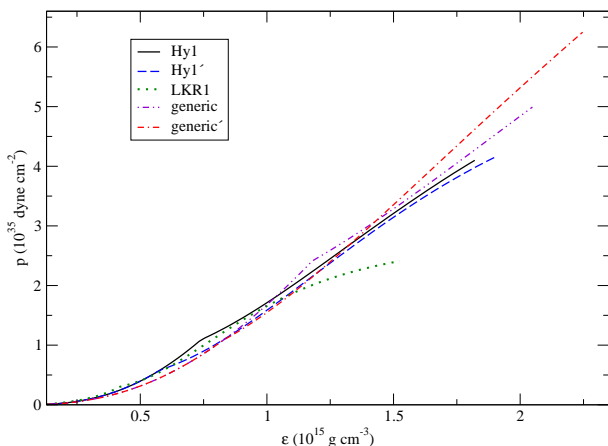


FIG. 1: Pressure vs. energy density for the EOSs from Table I, plotted up to the maximum energy density present in a stable OV star.

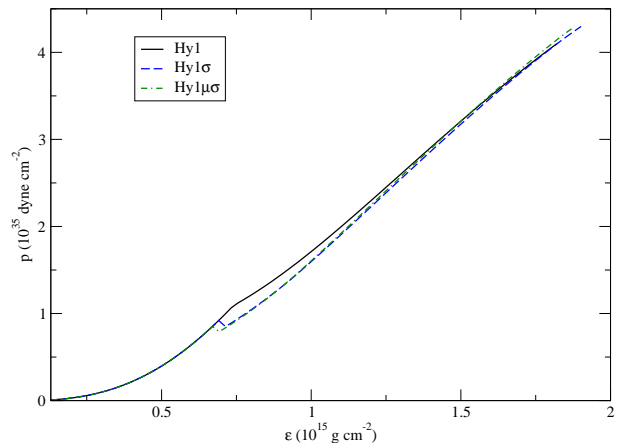


FIG. 2: Pressure vs. energy density for the Hy1 EOS and two flavors that include the surface tension contribution to the pressure balance, illustrating the violations of le Chatelier's principle. (Again, each of these is plotted up to the maximum energy density present in a stable OV star.)

A. Hadronic EOS

We construct the hadronic EOS following the recipe described in Chap. 4 of Glendenning's book [16] through Sec. 4.9. We thus use a relativistic mean field description, with a Lagrangian that contains the standard scalar and vector (σ and ω) fields, as well as scalar self-interactions, and the isospin asymmetry force, mediated by the vector meson ρ . We include neutrons, protons, electrons, and muons. See [25] and [58] for further details about the general framework and calculational procedure we used. However, we have used updated parameters in the models, as discussed above. Note that these references also consider hyperons, which we do not include in the EOSs considered here. In particular, hyperons and the hadron-quark mixed phase have been found to be mutually exclusive in some studies (see, e.g., [21, 59]).

The model has five input parameters: Two are known reasonably well, viz., the number density and binding energy per nucleon of nuclear matter at saturation, $n_0 = 0.16 \pm 0.01 \text{ fm}^{-3}$ and $(E/A)_{\infty} = -16 \pm 1 \text{ MeV}$. The remaining three are not nearly so well known: The nuclear incompressibility K is thought to lie between 200 and 300 MeV, with many authors placing it in the range $240 \pm 10 \text{ MeV}$ (see [60]), while the (scaled) Dirac effective mass of the nucleons, m^*/m , is thought to be between ~ 0.53 and 0.96 . (Here $m = 938.93 \text{ MeV} = 4.7582 \text{ fm}^{-1}$ is the average of the neutron and proton masses.) The symmetry energy a_{sym} is thought to lie between 28 and 34 MeV (see Li *et al.* [61]).

All parameter ranges are taken from Eq. (88) in Steiner *et al.* [62] unless otherwise noted. The range for the Dirac effective mass is computed from that for the Landau effective mass given by Steiner *et al.*, following Glendenning's Eq. (4.117) [16], with a Fermi momentum

	n_0 fm ⁻³	$(E/A)_\infty$ MeV	K MeV	m^*/m	a_{sym} MeV	$B^{1/4}$ MeV	α_s	$\bar{\Lambda}_{\text{QCD}}$ MeV	m_s MeV	σ MeV fm ⁻²	M_{max} M_\odot	$M_{\text{min}}^{\text{hybrid}}$ M_\odot	$R_{\text{max}}^{\text{hybrid}}/R$ %	C_{max}	densest hybrid phase
Hy1	0.153	-16.3	300	0.7	32.5	180	0.6	300	150	10, 20, 50, 80	2.057	1.747	58.1	0.486	Q, $d = 1.00$
Hy1 μ	0.153	-16.3	300	0.7	32.5	180	0.6	$\bar{\mu}_q$	150	80	2.061	1.716	59.5	0.487	Q, $d = 1.01$
Hy1 σ	0.153	-16.3	300	0.7	32.5	180	0.6	300	150	80, p	1.997	1.583	63.5	0.480	Q, $d = 1.00$
Hy1 $\mu\sigma$	0.153	-16.3	300	0.7	32.5	180	0.6	$\bar{\mu}_q$	150	80, p	2.000	1.545	64.9	0.481	Q, $d = 1.00$
Hy1'	0.153	-16.3	300	0.7	32.5	170	0.6	300	150	80	1.973	1.377	69.3	0.476	H, $d = 1.51$
LKR1	0.148	-16.3	271.76	0.6	37.4	167.5	0.6	300	100	80	1.955	1.096	72.4	0.433	H, $d = 3.00$
generic	0.16	-16	250	0.745	30	200	0.5	$\bar{\mu}_q$	100	80	1.986	1.878	44.0	0.500	Q, $d = 2.10$
generic'	0.16	-16	250	0.745	30	170	0.7	$\bar{\mu}_q$	100	80	1.974	1.534	65.7	0.513	Q, $d = 1.39$

TABLE I: EOS parameters and properties of their associated OV stars. In the $\bar{\Lambda}_{\text{QCD}}$ column, $\bar{\mu}_q$ denotes the cases where we take the QCD renormalization scale to be given by the average quark chemical potential at each density, as discussed in Sec. II B. In the σ column, we have denoted the cases in which we include the surface tension contribution to the pressure balance by a “p.” $M_{\text{min}}^{\text{hybrid}}$ gives the masses of stars that first contain hybrid matter; $R_{\text{max}}^{\text{hybrid}}/R$ denotes the maximum radius fraction occupied by hybrid matter (i.e., the radius fraction for the maximum mass star); and C_{max} denotes the maximum compactness ($2GM/Rc^2$) of a star. We also give the composition of the rare phase (“Q” for quark and “H” for hadronic) and the dimension of the lattice at the center of the maximum mass star. See the text for the definitions of other parameters.

at saturation of $1.33 \pm 0.03 \text{ fm}^{-1}$, from the Steiner *et al.* result and Glendenning’s Eq. (4.110).

Note that almost all of the NL3 parameters from LKR fall outside of the ranges we have given. We still consider them for two reasons. First, the LKR NL3 EOS is often treated as the paradigmatic stiff hadronic EOS in the literature; in particular, we were inspired to consider these parameters by the LKR EOS’s recent use in Weissenborn *et al.* [20]. Second, the LKR NL3 parameters are still regarded as providing an excellent fit to the nuclear binding energy and charge radius, explaining why this EOS remains in use.

B. Quark EOS

The quark matter is described by the MIT bag model (first given in Chodos *et al.* [63], and discussed briefly in Glendenning [16]), to capture the basic physics of confinement. This is supplemented with first-order QCD corrections to the thermodynamic potential for free quarks from Farhi and Jaffe [64], as described in Chap. 8 of Glendenning [16].² We take all the quarks to be massive (as opposed to the usual treatment in which only the strange quark is taken to be massive—see, e.g., [20, 65, 66]—but note that Christiansen and Glendenning [67] also take all three quarks to be massive). See Chap. 6 in [25] for further details of the calculation.

Here the parameters are all quite uncertain. The only firm constraint is that nonstrange quark matter is not absolutely stable, since this contradicts the observed existence of nuclei composed of nucleons. In addition, we assume that strange quark matter is not absolutely stable, since we consider hybrid stars, not strange stars. In

the pure bag model (with no QCD corrections—i.e., with zero QCD coupling constant), this implies that the fourth root of the bag constant, $B^{1/4}$, is greater than 145 MeV. When one includes QCD corrections, the minimum bag constant decreases—see, e.g., the discussion in Alford *et al.* [65]. There is no known upper bound on B , though for sufficiently large values of B (with all other EOS parameters fixed), stable stars do not contain deconfined quark matter.

We also need to know the QCD coupling constant and quark masses at the energy scale $\bar{\Lambda}_{\text{QCD}}$ at which we renormalize the perturbative contributions to the thermodynamic potential. This energy scale is typically taken to be the scale of the quark chemical potentials in the problem. Glendenning uses 300 MeV, though we find that the chemical potentials in the situations we consider are somewhat higher (up to ~ 480 MeV in the densest regions of stable stars). Therefore we also consider a density-dependent renormalization scale, given by $\bar{\Lambda}_{\text{QCD}} = \bar{\mu}_q := (\mu_p + \mu_n)/6$, where μ_p and μ_n are the proton and neutron chemical potentials, respectively, so $\bar{\mu}_q$ is an average quark chemical potential. (This was inspired by the chemical potential-dependent renormalization scale used in [66], though the specifics of their treatment differ.)

At this scale, the QCD coupling constant α_s is large and not well known (see Fig. 1 in [66] for the results from running the coupling constant using relatively low-order beta function expressions). We have considered values between 0.5 and 0.7, which are quite middle-of-the-road (particularly compared with the naïve beta function result of much greater than 1, though there is evidence that the QCD coupling constant “freezes” to a value of less than 1 at low energies—see, e.g., [68, 69]). Weissenborn *et al.* [20] consider values from 0 to 0.94,³ while

² Note that Glendenning corrects a sign error in Farhi and Jaffe’s result for the thermodynamic potential in his Eq. (8.14).

³ This is converted from Weissenborn *et al.*’s range of 0.4 to 1

Nayyar [25] uses values of 0.45 and 0.6. The quark masses are similarly uncertain. There are significant uncertainties (up to $\sim 50\%$) even at the 2 GeV scale at which the Particle Data Group [70] quotes the masses, and additional uncertainties in running them to lower energies. For simplicity, we have taken the up, down, and strange quarks to have masses of 2.5, 5, and 100 MeV, respectively, around the median of ranges for the $\overline{\text{MS}}$ current masses at 2 GeV given in the 2010 Review of Particle Physics [70]. We also consider a few cases with a strange quark mass of 150 MeV, for continuity with Nayyar [25].

C. Hybrid phase and its lattice structure

We determine the bulk properties of the mixed phase using the Gibbs equilibrium conditions, following Glendenning (see, e.g., Chap. 9 in [16]): The appearance of the mixed phase at a certain baryon number density is signaled by pure quark matter having a larger pressure than hadronic matter. We then determine the volume fractions of the two coexisting phases by demanding the equality of the phases' pressures and chemical potentials, in addition to global electrical neutrality. We compute the mixed-phase bulk pressure, energy, and baryon densities by weighting the contributions from each phase using their volume fractions.

We also need to obtain the crystalline structure of the mixed phase. This requires knowing the surface tension σ of the hadron–quark interface. While σ has been estimated very roughly in the literature (e.g., [64] and the references given in Endo [40]), its value is still quite uncertain, so we simply take it to range from 10 to 80 MeV fm $^{-2}$. (The lower bound is the default value used by Nayyar [25], and the upper bound is the default value used by Glendenning [16].) We make sure that it does not make an appreciable contribution to the overall energy density, since, as Glendenning discusses, the system's energy should not increase upon opening up a new degree of freedom. In the cases we have considered, the blobs' energy density is $\lesssim 2\%$ of the total. Similarly, the lattice's electrostatic pressure is also $\lesssim 3\%$ of the bulk pressure.

Although the Coulomb and surface energy of the blobs is only a small contribution to the overall energy density, it can still be significant compared to the energy difference between the pure hadronic phase and the mixed phase at a given baryon density, particularly at lower densities. Thus, as discussed by Heiselberg, Pethick, and Staubo [24] and Alford *et al.* [71], for sufficiently high surface tensions, the mixed phase may be disfavored compared to the sharp transition predicted by the Maxwell

construction. Christiansen and Glendenning, however, argue that the Maxwell construction should always correspond to an excited state for a multi-component system such as we are considering, and if any models predict otherwise for certain parameter values, they are not accurate for those parameters [67, 72].

Regardless, these energy arguments are all local (i.e., at a fixed baryon density). If one considers the energy of the star as a whole (at a fixed total baryon number), then the mixed phase can still be favored, particularly if one accounts for the increase of the star's own gravitational binding energy due to the attendant softening of the EOS at high densities. We shall present our analysis of the extent to which the mixed phase is present in stable stars for various surface tensions when we consider the associated maximum quadrupoles in [36]. Suffice it to say that given all the uncertainties present in these calculations, we still feel comfortable quoting results for surface tensions of 80 MeV fm $^{-2}$, at least as an indication of the upper bounds possible for the shear modulus. (We also discuss the dependence of the shear modulus on surface tension in Sec. VI.) Note that if one includes the lattice contributions to the EOS (energy density and pressure, plus the energy density of the blobs themselves), one obtains surface tension-dependent corrections to the values for stellar properties given in Table I. However, these are at most a few percent for the surface tensions we consider here.

Returning to the lattice structure, we note that the competition between the aforementioned surface tension and the Coulomb energy of the charges, the charge breaks up into blobs, which will then form a lattice. In order to determine the properties of this lattice, we employ the Wigner-Seitz approximation, which divides the lattice up into noninteracting, electrically neutral cells (approximating the lattice's Voronoi cell by a sphere of equivalent volume). Each cell contains a charged blob at its center surrounded by an equal amount of compensating charge. At lower densities, the blob is formed out of quark matter, and the hadronic matter provides the compensating charge; at higher densities—not reached in stable stars for many EOSs—the roles are reversed. The ratios of the volumes of the blob and the cell are fixed, since the baryon and quark volume fractions are fixed. If we denote the volume fraction of the rare phase by x , then we have $x = (r/R)^d$, where r and R are the radii of the blobs and cells, respectively (the half-thickness of the slabs in the one-dimensional case), and d is the dimensionality of the cell and lattice. If we denote the volume fraction of the quark phase by χ , we have

$$x = \begin{cases} \chi, & \chi \leq 1/2, \\ 1 - \chi, & \chi > 1/2. \end{cases} \quad (1)$$

We then determine r and d by minimizing the cell's energy per unit volume.

Following the suggestion initially made by Ravenhall, Pethick, and Wilson [23] in the nuclear pasta case, we

for Alford *et al.*'s a_4 [65] using the massless quark expression of $\alpha_s = (1 - a_4)\pi/2$ [cf. Eq. (3) in Alford *et al.* [65] and Eq. (6.4) in Nayyar [25]].

take the lattice's dimension to be a continuous variable. In the integer dimension cases, we have A_d^* : a body-centered cubic (bcc) lattice of spherical drops in 3 dimensions, a hexagonal lattice of cylindrical rods in 2 dimensions, and equally spaced rectangular slabs in 1 dimension. (These lattices are seen in the molecular dynamics simulations of nuclear pasta [42–45]. In particular, Watanabe *et al.* [43] obtain a hexagonal lattice of rods by adiabatically compressing a bcc lattice of drops in their molecular dynamics simulations.)

The expression for the energy per unit volume of a cell is then given by [Eqs. (9.19), (9.23), and (9.24) in Glendenning [16]]

$$\frac{E_{\text{cell}}}{\Omega} = C(x)r^2 + \frac{S(x)}{r}, \quad (2)$$

where Ω is the cell volume, and $C(x)$ and $S(x)$ correspond to the Coulomb and surface contributions, respectively, with

$$C(x) := 2\pi[(q_H - q_Q)(\chi)]^2 x f_d(x), \quad S(x) := x\sigma d. \quad (3)$$

Here q_H and q_Q are the hadron and quark charge densities and

$$f_d(x) := \frac{1}{d+2} \left[\frac{2 - dx^{1-2/d}}{d-2} + x \right]. \quad (4)$$

The singularity at $d \rightarrow 2$ is removable, since the limit exists [and has the expected value; see Eq. (9.30) in Glendenning [16]]. One can now immediately read off the minimizing r [Eq. (9.27) in Glendenning [16]], viz.,

$$r = \left[\frac{S(x)}{2C(x)} \right]^{1/3}. \quad (5)$$

One then obtains $d \in [1, 3]$ by minimizing (over that range) the resulting expression for the cell energy (using the minimizing r), viz., $E_{\text{cell}}/\Omega = (3/2)[2C(x)]^{1/3}[S(x)]^{2/3}$ [see Eq. (9.28) in Glendenning [16] for an explicit expression in terms of x , etc.]. We show the dependence of blob radius and lattice spacing [given in Eq. (49)] on χ for a few representative EOSs in Fig. 3. (The blob radii and lattice spacings of the three EOSs shown span the range covered by the entire set of EOSs in Table I.)

As discussed in, e.g., [37–40], the surface tension contributes to the pressure equality. Explicitly, we have a pressure difference between the dominant and rare phases of [cf. Eq. (A5) in [67]]

$$p_{\text{dominant}} - p_{\text{rare}} = \frac{(d-1)\sigma}{r}, \quad (6)$$

where r is the radius of the blobs. We have included this in our treatment of certain EOSs, though in a somewhat simplified version, so that it is numerically tractable. One obtains these EOSs by solving the appropriate equations at progressively larger and larger baryon densities (as

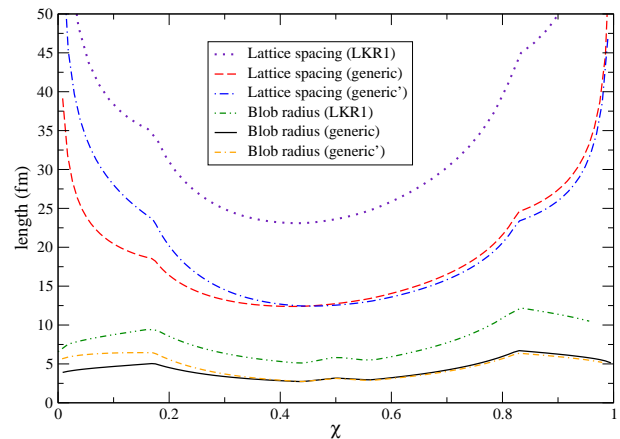


FIG. 3: The blob radius and lattice spacing versus χ for three representative EOSs.

discussed by Glendenning [16]). Our simplification consists of taking the lattice's dimension at a given baryon density to be fixed at the value obtained at the previous baryon density (instead of solving for the dimension including the dimension-dependent surface tension contribution to the pressure equality). Since this correction to the pressure equality is largest at the lowest-density portions of the mixed phase (i.e., the quark drop portions, with $d = 3$), our procedure for d seems likely to account for the primary effects from the surface tension's contribution to the pressure equality. (Note that we take the bulk pressure to be that of the dominant phase.)

With this treatment of the surface tension contribution to the pressure equality, we find a slight violation of le Chatelier's principle (i.e., monotonic increase of pressure with energy density) close to the hybrid transition. This is not present if one does not include the surface tension contribution to the pressure equality (see Fig. 2). Note that our method of solving the OV equations—using the enthalpy form given by Lindblom [73]—does not allow for such violations of le Chatelier's principle, since it requires one to express the energy density as a function of the pressure. We nonetheless quote results using the “smoothed-out” version of the EOS produced by MATHEMATICA's interpolation, feeling that they still give a reasonably accurate depiction of the star's bulk properties, since the violations of le Chatelier's principle we are considering are small.

D. Charge screening

The previous discussion has assumed that the charge is uniformly distributed within each blob and in the neutralizing background. This is not the case, in practice: The minimum-energy configuration will have a nonuniform charge distribution, as is discussed in, e.g., [37–39]. This nonuniform charge distribution—often treated in

the perturbative regime as charge screening—will affect the cell energy (and thus the lattice properties, for a given energy density), as well as the lattice’s electrostatic energy, and both of these affect the shear modulus. Here we only consider the effects on the lattice’s electrostatic energy due to linear charge screening of point charges, using a screened potential. As is commonly done in treatments of the mixed phase (e.g., those by Glendenning), we do not concern ourselves at all with the rearrangement of charge inside the blobs, though this is likely a significant effect (as is discussed in [37–39]).

In this linearized version, we treat screening as a small perturbation on the overall energy, leading to the expression for the Debye length given in Eq. (1) of [24], viz.,

$$\lambda = \left[4\pi \sum_{\alpha} Q_{\alpha}^2 \left(\frac{\partial n_{\alpha}}{\partial \mu_{\alpha}} \right) \right]^{-1/2}. \quad (7)$$

Here Q_{α} , n_{α} , and μ_{α} are the charge, number density, and chemical potential of particle species α , and the partial derivative is evaluated holding the chemical potentials of all species besides the α th fixed.

To include the effects of charge screening on the electrostatic energy, we dimensionally continue the standard screened potential equation (Yukawa in three dimensions), viz.,

$$(\Delta_d - \lambda^{-2})\phi = -4\pi Q\delta^{(d)}, \quad (8)$$

where Δ_d is the d -dimensional Laplacian, Q is the charge of the blob, and $\delta^{(d)}$ is the d -dimensional Dirac delta distribution.

The resulting potential is

$$\phi(r) = \frac{2Q}{(2\pi\lambda r)^{d/2-1}} K_{d/2-1}(r/\lambda), \quad (9)$$

where K_{ν} is the modified Bessel function of the second kind of order ν . This expression can be obtained most easily by noting that it is the same as the Euclidean scalar propagator (up to overall factors), which is given in a dimensionally continued form in Eq. (5) of [74].⁴

This potential clearly represents a simplified treatment of charge screening even in the perturbative limit, since we have used a point charge, instead of the extended charge distribution of a realistic blob with different screening lengths inside and outside. (We similarly use point charges when calculating the potential energy of other blobs due to this screened potential.) However, it is a practical way for us to account for some of the effects of charge screening. Since we are using this point charge approximation, we compute the screening length using the leptons and the background phase. This is because the rearrangement of charge within the blob has no

effect on the blob’s electrostatic potential except through the effects of screening on the blob’s size, which we are ignoring here. This switch at $\chi = 1/2$ causes a significant jump in the screening length there. This translates into a jump in the elastic constants, and thus the effective shear modulus, as seen in the figures in Sec. VI. The magnitude of this jump gives some indication of the overall error we incur through our simplified treatment of charge screening in the potential. (However, this likely does not give any indication of the errors incurred by neglecting the contribution of charge screening to the cell energy, which we shall see affects the effective shear modulus both directly and indirectly.)

III. ELASTICITY

The elastic response of a crystalline lattice is described by its elastic modulus tensor, S_{klps} , defined by

$$\mathcal{E} = \mathcal{E}_0 + S_{kl}u_{kl} + \frac{1}{2}S_{klps}u_{kl}u_{ps}, \quad (10)$$

where \mathcal{E} is the deformed lattice’s energy density, \mathcal{E}_0 is its undeformed energy density, $u_{kl} := \partial_k \delta x_l$ is the displacement gradient (where δx_l denotes the displacement field), and S_{kl} is the first-order piece of the expansion. We have a nonzero first-order piece here, since the undeformed lattice has a nonzero pressure—see Eq. (7) in Baiko [49]. (Wallace [75] gives further discussion.) Explicitly, we have $S_{kl} = -P_{\text{es}}\delta_{kl}$, since the pressure is isotropic. (Note that we shall only consider the contribution from the lattice’s electrostatic pressure P_{es} in our discussion.) Now, we are only interested in the shear stress the lattice generates in response to a shear deformation, and this is given by a different elastic modulus tensor, viz.,

$$B_{klps} = S_{klps} - P_{\text{es}}(\delta_{ks}\delta_{lp} - \delta_{kl}\delta_{ps}). \quad (11)$$

Specifically, the stress generated by a deformation u_{kl} is given by $B_{klps}(u_{ps} + u_{sp})/2$. [See Eqs. (29) and (30) in Baiko [49].] We can write the components of B_{klps} more simply by using Voigt notation to map them to the two-index object $c_{\alpha\beta}$ using the index mapping given by $\{xx, yy, zz, xy, xz, yz\} \leftrightarrow \{1, 2, 3, 4, 5, 6\}$ where (x, y, z) are Cartesian coordinates. With this notation, we have $c_{11} = S_{1111}$ and $c_{44} = S_{1212}$, while $c_{12} = S_{1122} + P_{\text{es}}$. [Note that Baiko’s C_{kl} denotes a different tensor.]

Since we are interested solely in the lattice’s response to shears, we can focus our attention on a few components of this tensor. If we just consider the cases where a shear strain yields a proportional shear stress (as is the case for isotropic materials), then we will have contributions from the simple shear portions of the tensor, viz., c_{44} , c_{55} , and c_{66} , in addition to the elongational shears $A_{12} := (c_{11} + c_{22})/2 - c_{12}$, $A_{13} := (c_{11} + c_{33})/2 - c_{13}$, and $A_{23} := (c_{22} + c_{33})/2 - c_{23}$. The simple shears correspond to stresses or strains of the form $2\hat{x}_{(k}\hat{y}_{l)}$ where \hat{x}_k

⁴ When comparing the two expressions, note that $K_{-\nu} = K_{\nu}$.

and \hat{y}_k are unit vectors in the x - and y -directions, and parentheses on the indices indicate symmetrization. The elongational shears correspond to stresses or strains of the form $\hat{x}_k \hat{x}_l - \hat{y}_k \hat{y}_l$ —i.e., rotations of the simple shears by $\pi/4$. In the past, some investigations of shear modulus effects in the crusts of neutron stars have used the simple shear portion of the tensor, c_{44} , as the shear modulus of a bcc lattice (for which $c_{44} = c_{55} = c_{66}$)—see the discussion in Sec. 7.1 of Chamel and Haensel [76]. As Strohmayer *et al.* [77] emphasize, it is inappropriate to simply use one component of the elastic modulus tensor for this purpose. While a truly detailed calculation would use the full elastic modulus tensor, if one considers a polycrystal consisting of many randomly oriented domains, it is possible to use an angle-averaged version of the shear portions of this tensor and obtain an upper bound.

This upper bound is due to Voigt [78], and involves the elastic constants given above—see Hill [79] for the proof that the Voigt expression gives an upper bound. We do not consider any of the more involved sharper bounds, such as the oft-used ones by Hashin and Shtrikman [80]. (See [81] for a review of such bounds, and [82] for a Hashin-Shtrikman bound for orthorhombic crystals, such as the ones we consider here.) The Voigt result was rediscovered by Ogata and Ichimaru [83] in considering the shear modulus of the neutron star crust. (They used it as an average, as was originally proposed by Voigt, not as an upper bound, as in Hill.) Following Ogata and Ichimaru [83] and most subsequent work, we shall use the Voigt average for our effective shear modulus, giving

$$\mu_{\text{eff}} = (A_{12} + A_{13} + A_{23})/15 + (c_{44} + c_{55} + c_{66})/5. \quad (12)$$

We note, as does Baiko [49], that the lattice will likely tend to align itself with the star’s magnetic field, leading to a large-scale ordered structure. However the standard averaging approach we use here is a necessary first step, and may be a good approximation to bulk properties of the star if the internal magnetic field lines are tangled as in some simulations such as Braithwaite and Spruit [84].

To dimensionally continue this expression, we need to consider the effects of different lattice dimensionalities on the shear elastic coefficients. We shall first discuss the integer dimension cases, and then present the dimensionally continued expression for the effective shear modulus at the end. (See Pethick and Potekhin [41] for related discussion about the elasticity of liquid crystals as applied to the pasta phases in the crust.) Our discussion will be simplified by the fact that we can take the elastic constants of all the lattices to have cubic symmetry—this holds for the integer dimension lattices and remains true for the dimensionally continued ones by fiat. However, there will be differences between the elongational shear elastic constants in which the shear takes place completely within the lattice and those that involve an elongation along the rods or slabs. We also will find that the number of nonzero shear elastic constants is reduced due to the translational symmetry along the rods or slabs

in lower dimensions. Specifically,

1. In the three-dimensional case, all the shear elastic constants are nonzero, and, by cubic symmetry, the simple and elongational shear elastic constants are each all equal (i.e., $c_{44} = c_{55} = c_{66}$ and $A_{12} = A_{13} = A_{23} =: A_{\text{lat}}$).
2. In the two-dimensional case, only one of the simple shear elastic constants is nonzero, since simple shears along the rods do not lead to a shear stress—i.e., we have $c_{66} \neq c_{44} = c_{55} = 0$, where we have taken the rods to point in the z -direction. The elongational shears are all nonzero, but are not all equal: In general, the one elongational shear perpendicular to the rods (i.e., within the lattice, so denoted A_{lat}) has a different elastic constant than do the two elongational shears that involve elongations along the rods (i.e., perpendicular to the lattice, and so denoted A_{\perp}). Explicitly, we have $A_{\text{lat}} := A_{12} \neq A_{13} = A_{23} =: A_{\perp}$.
3. In the one-dimensional case, all of the simple shear elastic constants are zero, due to the translational symmetry along the slabs, and the only nonzero elongational shear constants are those that involve elongation along the slabs. (We neglect any change in energy due to shearing one of the slabs.) We thus have $c_{44} = c_{55} = c_{66} = 0$ and, taking the x -direction to be perpendicular to the slabs, $A_{\text{lat}} := A_{12} = A_{13} \neq A_{23} = 0$.

We can now obtain the dimensionally continued version by using the dimensionally continued versions of the relevant basic combinatorial results: The number of independent shears (either simple or elongational) completely within the lattice (i.e., perpendicular to the rods and slabs in the integer dimension cases) is given by $d(d-1)/2$; this gives the multiplicity of the contributions to μ_{eff} from c_{44} and A_{lat} . The number of independent elongational shears with one elongation perpendicular to the lattice and one within it is given by $d(3-d)$; this gives the multiplicity of the contributions from A_{\perp} . The dimensionally continued version of Eq. (12) is thus

$$\mu_{\text{eff}} = \frac{d}{15} \left[\frac{d-1}{2} A_{\text{lat}} + (3-d) A_{\perp} \right] + \frac{d(d-1)}{10} c_{44}. \quad (13)$$

IV. CALCULATION OF THE ELASTIC CONSTANTS

Now looking at how to compute A_{lat} , A_{\perp} , and c_{44} , we can follow Fuchs [48] in expressing these quantities in terms of lattice sums. Specifically, we write the electrostatic energy of an appropriately deformed lattice as a lattice sum and takes derivatives with respect to the deformation to obtain lattice sum expressions for the elastic constants. In A_{\perp} , we will also need to consider the contributions from the cell energy [obtained using Eq. (2)].

One also expects there to be contributions to A_{lat} and c_{44} due to changing the shape of the unit cell [67, 85], but we neglect these in our treatment. We do not have to concern ourselves with such contributions for A_{\perp} , even in principle, since we can take the compression inside the lattice to be uniform in all directions.

We also follow Fuchs in using the Ewald method to compute the resulting lattice sums. (See, e.g., [47] for a modern exposition of the Ewald method. Additionally, we make certain modifications to the method so that it is compatible with dimensional continuation—these are discussed in Sec. V A.) In the Ewald method, one computes the sum of a slowly convergent or divergent series by expressing it as the sum of two rapidly convergent series, introducing an Ewald screening function and using the Poisson summation formula. (Actually, the Poisson summation formula is not strictly applicable to the functions being summed in many applications, which is what allows the Ewald method to regularize divergent series, by much the same method as zeta function regularization—see the Appendix for further discussion.)

The Fuchs expressions are obtained by computing the energy of the perturbed lattice. Explicitly, we write the electrostatic energy per unit cell of the lattice (i.e., the energy required to remove a single blob) as

$$W = \frac{Q^2}{2} \left[\sum'_{\vec{x} \in \Lambda} (\phi E)(\|\vec{x}\|) + \frac{1}{\Omega} \sum'_{\vec{p} \in \Lambda^*} (\widehat{\phi E_c})(\|\vec{p}\|) - \frac{(\widehat{\phi E})(0)}{\Omega} \right]. \quad (14)$$

$$\begin{aligned} \mathfrak{c} = \frac{Q^2}{2\Omega} & \left\{ \sum'_{\vec{x} \in \Lambda} \left[(\phi E)'(\|\vec{x}\|) \frac{\partial^2 \|\vec{x}\|}{\partial \epsilon^2} + (\phi E)''(\|\vec{x}\|) \left(\frac{\partial \|\vec{x}\|}{\partial \epsilon} \right)^2 \right] + \frac{1}{\Omega} \sum'_{\vec{p} \in \Lambda^*} \left[2 \frac{(\widehat{\phi E_c})(\|\vec{p}\|)}{\Omega^2} \left(\frac{\partial \Omega}{\partial \epsilon} \right)^2 \right. \right. \\ & \left. \left. + (\widehat{\phi E_c})^{\bullet}(\|\vec{p}\|) \left(\frac{\partial^2 \|\vec{p}\|^2}{\partial \epsilon^2} - \frac{2}{\Omega} \frac{\partial \Omega}{\partial \epsilon} \frac{\partial \|\vec{p}\|^2}{\partial \epsilon} \right) + (\widehat{\phi E_c})^{\bullet\bullet}(\|\vec{p}\|) \left(\frac{\partial \|\vec{p}\|^2}{\partial \epsilon} \right)^2 \right] - \frac{2}{\Omega^3} \left(\frac{\partial \Omega}{\partial \epsilon} \right)^2 (\widehat{\phi E})(0) \right\} \Bigg|_{\epsilon=0}, \end{aligned} \quad (15)$$

where the coordinate and Ω derivatives are given by Eqs. (16) and (17). [Recall that Ω is unchanged by the c_{44} perturbation.] The superscript bullets (\bullet) denote derivatives taken with respect to $\|\vec{p}\|^2$ —cf. the discussion below Eq. (16).

To obtain the derivatives needed for the lattice sum expression for c_{44} , we note (following Fuchs [48]) that c_{44} is the only elastic constant that contributes to the change of energy of the lattice if one considers a simple shear deformation. If we take this simple shear to be in the x_1 and x_2 directions [now denoting our Cartesian coordinates by (x_1, x_2, x_3) , instead of the previous (x, y, z) , for notational convenience], it corresponds to the deformations $x_1 \rightarrow x_1 + \epsilon x_2$, $x_2 \rightarrow x_2 + \epsilon x_1$ for the direct lattice, and $p_1 \rightarrow (p_1 - \epsilon p_2)/(1 - \epsilon^2)$, $p_2 \rightarrow (p_2 - \epsilon p_1)/(1 - \epsilon^2)$ for the dual lattice (x_3 and p_3 are both held fixed). The

[Compare the expression for the potential in Eq. (7) of Johnson and Ranganathan [47] and Fuchs's expression for the energy in Eq. (10) of [48].] Here Q is the charge of a blob; Λ is the lattice under consideration, with dual lattice Λ^* , and physical Voronoi cell volume Ω . We shall also use Conway and Sloane's [51] notation of $\sqrt{\det \Lambda}$ for the Voronoi cell volume without the physical scaling. Primes on the sums denote the omission of the zero vector; E is the Ewald screening function, with complement $E_c(x) := 1 - E(x)$; ϕ is the potential due to one of the blobs [including the effects of (physical) charge screening]; and the circumflex denotes the Fourier transform of (here three-dimensional) radial functions. (See Sec. V A for our Fourier transform conventions.)

We now give the lattice sum expressions for the elastic constants. The most straightforward are those for c_{11} and c_{44} , which are of the form $(d^2 W / d\epsilon^2)|_{\epsilon=0} / \Omega$, for an appropriate deformation parametrized by ϵ . (Note that we need c_{11} in order to compute A_{\perp} and the dimensionally continued A_{lat} , even though that elastic constant does not appear in μ_{eff} by itself.) The resulting expressions for elastic constants take the form ($\mathfrak{c} \in \{c_{11}, c_{44}\}$)

requisite derivatives are thus

$$\frac{\partial \|\vec{x}\|}{\partial \epsilon} \Bigg|_{\epsilon=0} = \frac{x_1 x_2}{\|\vec{x}\|}, \quad \frac{\partial^2 \|\vec{x}\|}{\partial \epsilon^2} \Bigg|_{\epsilon=0} = \frac{x_2^2}{\|\vec{x}\|} - \frac{x_1^2 x_2^2}{\|\vec{x}\|^3}, \quad (16a)$$

$$\frac{\partial \|\vec{p}\|^2}{\partial \epsilon} \Bigg|_{\epsilon=0} = 2p_1 p_2, \quad \frac{\partial^2 \|\vec{p}\|^2}{\partial \epsilon^2} \Bigg|_{\epsilon=0} = 2p_1^2. \quad (16b)$$

[*Nota bene* (N.B.): We have given the derivatives of $\|\vec{p}\|^2$ since the dimensionally continued Fourier transform depends naturally on this quantity—cf. Eq. (29). Additionally, all of the right-hand sides of these expressions are evaluated at $\epsilon = 0$ (both here and in all similar situations in the next equation).]

For c_{11} , we use the deformation $x_1 \rightarrow (1 + \epsilon)x_1$, $p_1 \rightarrow p_1/(1 + \epsilon)$ (with all other coordinates held fixed). This perturbation changes the cell volume, so we must include derivatives of Ω , giving

$$\left. \frac{\partial \|\vec{x}\|}{\partial \epsilon} \right|_{\epsilon=0} = \frac{x_1^2}{\|\vec{x}\|}, \quad \left. \frac{\partial^2 \|\vec{x}\|}{\partial \epsilon^2} \right|_{\epsilon=0} = \frac{x_1^2}{\|\vec{x}\|} - \frac{x_1^4}{\|\vec{x}\|^3}, \quad (17a)$$

$$\left. \frac{\partial \|\vec{p}\|^2}{\partial \epsilon} \right|_{\epsilon=0} = -2p_1^2, \quad \left. \frac{\partial^2 \|\vec{p}\|^2}{\partial \epsilon^2} \right|_{\epsilon=0} = 6p_1^2, \quad (17b)$$

$$\left. \frac{\partial \Omega}{\partial \epsilon} \right|_{\epsilon=0} = \Omega, \quad \left. \frac{\partial^2 \Omega}{\partial \epsilon^2} \right|_{\epsilon=0} = 0. \quad (17c)$$

For A_{lat} , Fuchs uses the elongational shear in the x_1 and x_2 directions, for which the change to the lattice's energy is given by $2A_{\text{lat}}$ alone (and has a lattice sum expression similar to that for c_{44}). However, as we shall see in Sec. V, the resulting expression is not well suited for dimensional continuation, since it contains fourth powers of more than one coordinate [see Eq. (12) in Fuchs [48]]. We can obtain an expression that *is* well-suited to dimensional continuation if we note that $A_{\text{lat}} = c_{11} - c_{12}$ (we have $c_{11} = c_{22}$ by cubic symmetry): We compute c_{11} as above, but obtain $c_{12} = S_{1122} + P_{\text{es}}$ by first using a two-component perturbation to obtain S_{1122} , and then computing P_{es} *à la* Fuchs. The two-component perturbation we use to obtain S_{1122} is $x_1 \rightarrow (1 + \epsilon_1)x_1$, $x_2 \rightarrow (1 + \epsilon_2)x_2$, $p_1 \rightarrow p_1/(1 + \epsilon_1)$, $p_2 \rightarrow p_2/(1 + \epsilon_2)$ (with x_3 and p_3 held fixed), yielding the derivatives

$$\left. \frac{\partial \|\vec{x}\|}{\partial \epsilon_j} \right|_{\epsilon_{1,2}=0} = \frac{x_j^2}{\|\vec{x}\|}, \quad \left. \frac{\partial^2 \|\vec{x}\|}{\partial \epsilon_1 \partial \epsilon_2} \right|_{\epsilon_{1,2}=0} = -\frac{x_1^2 x_2^2}{\|\vec{x}\|^3}, \quad (18a)$$

$$\left. \frac{\partial \|\vec{p}\|^2}{\partial \epsilon_j} \right|_{\epsilon_{1,2}=0} = -2p_j^2, \quad \left. \frac{\partial^2 \|\vec{p}\|^2}{\partial \epsilon_1 \partial \epsilon_2} \right|_{\epsilon_{1,2}=0} = 0, \quad (18b)$$

$$\left. \frac{\partial \Omega}{\partial \epsilon_j} \right|_{\epsilon_{1,2}=0} = \Omega, \quad \left. \frac{\partial^2 \Omega}{\partial \epsilon_1 \partial \epsilon_2} \right|_{\epsilon_{1,2}=0} = \Omega, \quad (18c)$$

where $j \in \{1, 2\}$ and $\epsilon_{1,2} = 0 \Rightarrow \epsilon_1 = \epsilon_2 = 0$. One then obtains, from $S_{1122} = (\partial^2 W / \partial \epsilon_1 \partial \epsilon_2)|_{\epsilon_{1,2}=0} / \Omega$ and the expression for W in Eq. (14),

$$\begin{aligned} S_{1122} = & \frac{Q^2}{2\Omega} \left\{ \sum'_{\vec{x} \in \Lambda} \frac{x_1^2 x_2^2}{\|\vec{x}\|^2} \left[(\phi E)''(\|\vec{x}\|) - \frac{(\phi E)'(\|\vec{x}\|)}{\|\vec{x}\|} \right] \right. \\ & + \frac{1}{\Omega} \sum'_{\vec{p} \in \Lambda^*} \left[(\widehat{\phi E}_c)(\|\vec{p}\|) + 2(p_1^2 + p_2^2)(\widehat{\phi E}_c) \bullet (\|\vec{p}\|) \right. \\ & \left. \left. + 4p_1^2 p_2^2 (\widehat{\phi E}_c) \bullet \bullet (\|\vec{p}\|) \right] - \frac{1}{\Omega} (\widehat{\phi E})(0) \right\} \Big|_{\epsilon_{1,2}=0}. \end{aligned} \quad (19)$$

We calculate P_{es} using the same perturbation we used to obtain c_{11} [with the derivatives given in Eq. (17)]. Specifically, $P_{\text{es}} = - (dW/d\epsilon)|_{\epsilon=0} / \Omega$ [cf. Eq. (10), recall-

ing that $S_{kl} = -P_{\text{es}} \delta_{kl}$]. This gives

$$\begin{aligned} P_{\text{es}} = & -\frac{Q^2}{2\Omega} \left\{ \sum'_{\vec{x} \in \Lambda} \frac{x_1^2}{\|\vec{x}\|} (\phi E)'(\|\vec{x}\|) - \frac{1}{\Omega} (\widehat{\phi E})(0) \right. \\ & \left. - \frac{1}{\Omega} \sum'_{\vec{p} \in \Lambda^*} \left[(\widehat{\phi E}_c)(\|\vec{p}\|) + 2p_1^2 (\widehat{\phi E}_c) \bullet (\|\vec{p}\|) \right] \right\} \Big|_{\epsilon=0}. \end{aligned} \quad (20)$$

We thus have

$$A_{\text{lat}} = c_{11} - S_{1122} - P_{\text{es}}, \quad (21)$$

where c_{11} is given by Eqs. (15) and (17), and S_{1122} and P_{es} are given by the above expressions.

Now, to obtain A_{\perp} , we need to supplement the expression for c_{11} with the contributions due to changing the cell energy (since we are changing its radius), along with the contributions due to changing the blobs' charge. The contribution due to changing the cell energy is

$$A_{\perp, \text{cell}} = \frac{2}{d^2} \frac{E_{\text{cell}}}{\Omega}, \quad (22)$$

where E_{cell}/Ω is given in Eq. (2). This can be deduced from the scalings of the Coulomb and surface contributions [see Eq. (2) in Pethick and Potekhin [41]], noting that the change in the cell radius with this perturbation is given by

$$\left. \frac{\partial r}{\partial \epsilon} \right|_{\epsilon=0} = \frac{r}{d}, \quad (23)$$

which comes from noting that $\Omega = C_{\text{cell}} r^d$, where C_{cell} is a constant (since x is fixed, as we are keeping the overall density fixed) and $(\partial \Omega / \partial \epsilon)|_{\epsilon=0} = \Omega$ for the c_{11} perturbation. For the derivatives of the blobs' charge, we note that the (three-dimensional) charge density is fixed, so that the derivatives of the blobs' charge can be obtained from those of the cell volume [in Eq. (17c)] by replacing the cell volume with the blobs' charge. Explicitly, we have

$$\left. \frac{\partial Q}{\partial \epsilon} \right|_{\epsilon=0} = Q, \quad \left. \frac{\partial^2 Q}{\partial \epsilon^2} \right|_{\epsilon=0} = 0. \quad (24)$$

We now show how to put together all these contributions to obtain the sum that gives A_{\perp} : We have

$$A_{\perp} = c_{11} + A_{\perp, \text{cell}} + A_{\perp, Q}, \quad (25)$$

where c_{11} is given by Eqs. (15) and (17), $A_{\perp, \text{cell}}$ is given in Eq. (22), and

$$\begin{aligned} A_{\perp, Q} = & \frac{Q^2}{\Omega} \left\{ \sum'_{\vec{x} \in \Lambda} \left[(\phi E)(\|\vec{x}\|) + 2 \frac{x_1^2}{\|\vec{x}\|} (\phi E)'(\|\vec{x}\|) \right] \right. \\ & - \frac{1}{\Omega} \sum'_{\vec{p} \in \Lambda^*} \left[(\widehat{\phi E}_c)(\|\vec{p}\|) + 4p_1^2 (\widehat{\phi E}_c) \bullet (\|\vec{p}\|) \right] \\ & \left. + \frac{(\widehat{\phi E})(0)}{\Omega} \right\} \Big|_{\epsilon=0}. \end{aligned} \quad (26)$$

As one would expect from Earnshaw's theorem, c_{11} is always negative, so one relies on the contributions from $A_{\perp, \text{cell}}$ and $A_{\perp, Q}$ to make A_{\perp} positive so that the lattice is stable to shears. (See Sec. VI for further discussion.)

V. DIMENSIONAL CONTINUATION OF LATTICE SUMS

A. The dimensionally continued Ewald method

In order to compute these lattice sums numerically, we employ a generalization of the standard Ewald [46] method used by Fuchs [48]. Showing the standard integer dimension version first, we have, summing a function f over a lattice Λ with dual lattice Λ^* ,

$$\sum_{\vec{x} \in \Lambda} f(\vec{x}) = \sum_{\vec{x} \in \Lambda} (fE)(\vec{x}) + \frac{1}{\sqrt{\det \Lambda}} \sum_{\vec{p} \in \Lambda^*} (\widetilde{fE_c})(\vec{p}). \quad (27)$$

Here $E_c(\vec{x}) := 1 - E(\vec{x})$ is the complement of the Ewald screening function E , $\tilde{g}(\vec{p}) := \int_{\mathbb{R}^n} g(\vec{x}) e^{-2\pi i \vec{x} \cdot \vec{p}} d^n x$ denotes the standard Fourier transform, and we choose E so that both of the sums on the right-hand side converge quickly. [Recall that the classical Poisson summation formula says that $\sum_{\vec{x} \in \Lambda} f(\vec{x}) = (\det \Lambda)^{-1/2} \sum_{\vec{p} \in \Lambda^*} \tilde{f}(\vec{p})$.]

The classic choice for E for Coulombic potentials (dating back to Ewald) is the complementary error function. However, this turns out to be insufficiently flexible to provide good convergence for the sums we consider (particularly for small d). Following Nijboer and de Wette [86] and Fortuin [87], we introduce the incomplete gamma function, $\Gamma(\cdot, \cdot)$, and use the screening function

$$E(\vec{x}) = \Gamma(N/2, \alpha^2 \|\vec{x}\|^2) / \Gamma(N/2). \quad (28)$$

This reduces to Ewald's complementary error function for $N = 1$. The extra freedom contained in N allows us to tune E to provide fast convergence for the sums we encounter. We used $N = 10$ and $\alpha = 1.2/a$ in the computations reported in Sec. VI. [Here a is the lattice spacing, given in Eq. (49).] We could have doubtless obtained faster convergence if we had allowed these parameters to vary with d (and possibly also λ), particularly for d close to 1. However, we found that these values to give reasonably good performance, and thus did not perform much experimentation beyond checking that our results are insensitive to small variations in the Ewald screening parameters.

In order to dimensionally continue our lattice sums, we need to dimensionally continue the Poisson summation formula. We shall give an overview of the calculational aspects here—see [50] for more details of the derivations, and a proof of the formula for nicely behaved functions. We first introduce the dimensionally continued Fourier transform for spherically symmetric functions, given in Theorem 3.3 of Chap. IV of Stein and Weiss [88],

$$\hat{g}(p) := \frac{2\pi}{p^{d/2-1}} \int_0^\infty g(r) J_{d/2-1}(2\pi pr) r^{d/2} dr. \quad (29)$$

Here J_ν is the Bessel function of the first kind. (See Sec. 2.2 of [50] for more details, including an alternative expression in terms of a hypergeometric function.) We also note that we can compute the dimensionally continued Fourier transform of the potential from its defining partial differential equation (8), giving

$$\hat{\phi}_d(p) = \frac{4\pi}{4\pi^2 p^2 + \lambda^{-2}}. \quad (30)$$

[This agrees with the result of the more involved calculation one could perform using the dimensionally continued Fourier integral given in Eq. (29).] We use Eq. (30) along with the dimensionally continued Fourier integral (29) to compute $\widehat{\phi E_c}$ efficiently, writing it as $\hat{\phi} - \widehat{\phi E}$, where the integral giving the second term converges reasonably rapidly.

We then introduce the theta series of a lattice. As is discussed in more detail in Sec. 2.3 of Chap. 2 of Conway and Sloane [51], the theta series of a lattice is the generating function of the number of lattice points on a sphere of a given squared radius, so the theta series of a lattice Λ is defined by

$$\Theta_\Lambda(q) := \sum_{\vec{k} \in \Lambda} q^{\|\vec{k}\|^2}. \quad (31)$$

[N.B.: There are several different notational conventions for theta series and theta functions. We have chosen to write all our theta series and functions as functions of the nome, q , unless we note otherwise. These exceptions will only occur in discussions of the Jacobi formula for the theta series of the dual lattice, where it is convenient to treat the theta series as a function of a complex variable z , with $q = e^{i\pi z}$. We shall denote this by an overbar—e.g., $\bar{\Theta}_\Lambda(z) := \Theta_\Lambda(e^{i\pi z})$. Conway and Sloane treat all their theta functions as functions of z , even when they write their expansions in terms of the nome.] Thus, if we define the power series coefficients of the theta series using

$$\Theta_\Lambda(q) =: \sum_{l=0}^{\infty} A_l q^{B_l}, \quad (32)$$

we can write the sum of a spherically symmetric function F over Λ as

$$\sum_{\vec{k} \in \Lambda} F(\|\vec{k}\|) = \sum_{l=0}^{\infty} A_l F(\sqrt{B_l}). \quad (33)$$

The dimensionally continued Poisson summation formula then has the form

$$\sum_{l=0}^{\infty} A_l F(\sqrt{B_l}) = \frac{1}{\sqrt{\det \Lambda}} \sum_{l=0}^{\infty} A_l^* \hat{F}(\sqrt{B_l^*}). \quad (34)$$

Here, A_l^* and B_l^* are defined analogously to their counterparts for Λ . The theta series for Λ^* can be calculated from Θ_Λ using the Jacobi formula (39), which is

already in dimensionally continued form. [N.B.: The dimensionally continued Poisson summation formula presented in [50] omits the factor of $(\det \Lambda)^{-1/2}$, since, as discussed there, this factor cancels against a similar one present in the Jacobi transformation formula. We include the factor here, since we obtain a simpler result for the theta series of the dual lattice by using the standard Jacobi transformation formula.] Of course, we need to sum more than just spherically symmetric functions [see Eqs. (15)–(20)], but, as we shall see shortly, this dimensionally continued Poisson summation formula will be sufficient for our needs.

B. Dimensional continuation of the lattice

Turning now to the problem of dimensionally continuing the lattices themselves, recall that the integer dimension lattices are [up to an overall scaling, which we determine in Eq. (49)] a bcc lattice for $d = 3$, a hexagonal lattice for $d = 2$, and \mathbb{Z} , the (one-dimensional) lattice of integers, for $d = 1$. In some sense, the natural way to dimensionally continue these lattices would be to dimensionally continue the root lattice family A_d^* , which gives those lattices for $d \in \{1, 2, 3\}$ and, more generally, gives the best lattice covering of \mathbb{R}^n for $n \leq 5$ (as discussed in Conway and Sloane [51]). However, unlike most other families of lattices, A_d^* does not have a theta series that is written in a nicely dimensionally continued form. Its theta series is written in terms of a sum whose number of terms depends upon dimension—see, e.g., Eq. (56) in Chap. 4 of Conway and Sloane [51] for the theta series for A_d , from which the theta series for the dual lattice can be obtained using Jacobi’s formula [our Eq. (39)]. The sum is over d th roots of unity, so one could contemplate writing it as an integral, using Cauchy’s theorem, and proceeding that way. However, even disregarding the complications this would involve, it is not clear how to compute the sums involving x_1^4 that we need (for, e.g., c_{11}) in this framework, or, alternatively, how to implement the requisite distortions to the lattice at the level of its theta series.

We thus proceed by treating the dimensionally continued lattice as a union of hyperlattices (i.e., lattices of one dimension fewer than the overall lattice)⁵ whose separation is given by a freely specifiable function f^{lat} that interpolates between the integer dimension separations. One then finds that the sums over the hyperlattices dimensionally continue in a natural way, and that the final result for the shear modulus is rather insensitive to the choice of f^{lat} (provided that it satisfies some reasonable properties, discussed below).

Explicitly, the (scaled) integer dimension lattices can

be written as $[f^{\text{lat}}(d)\mathbb{Z}_{\text{even}}] \times \mathbb{Z}^{d-1} + [f^{\text{lat}}(d)\mathbb{Z}_{\text{odd}}] \times [\mathbb{Z}^{d-1} + (1/2)^{d-1}]$, where \mathbb{Z}_{even} and \mathbb{Z}_{odd} denote the even and odd integers respectively, \mathbb{Z}^{d-1} denotes the $(d-1)$ -dimensional lattice of integers, and $\mathbb{Z}^{d-1} + (1/2)^{d-1}$ denotes the same shifted by the $[(d-1)$ -dimensional] vector all of whose components are $1/2$. This is illustrated in Fig. 4, where we take x_1 to be in the direction orthogonal to the hyperlattices.

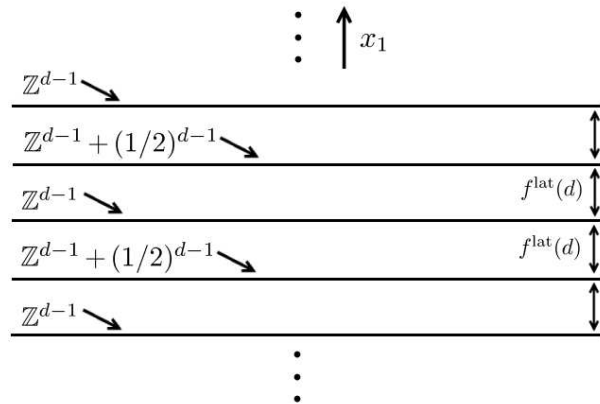


FIG. 4: A schematic of the decomposition of the full lattice into hyperlattices.

Here $f^{\text{lat}}(d)$ is freely specifiable, except that it must satisfy $\{1, 2, 3\} \mapsto \{1, \sqrt{3}/2, 1/2\}$. Additionally, it makes sense to choose it to be smooth, nonincreasing, and concave. A possibility that satisfies all these criteria is

$$f_{\cos}^{\text{lat}}(d) := \cos\left(\frac{\pi}{6}[d-1]\right), \quad (35)$$

which we will use in all our results, unless otherwise noted. We will show that the results for other possibilities all agree well with f_{\cos}^{lat} . Consider the envelope of all possible functions satisfying the requirements. The bounds on this envelope are

$$f_{\text{inf}}^{\text{lat}}(d) = \begin{cases} (\sqrt{3}/2 - 1)(d-1) + 1, & 1 \leq d < 2, \\ [(1 - \sqrt{3})(d-2) + \sqrt{3}]/2, & 2 \leq d \leq 3, \end{cases} \quad (36a)$$

$$f_{\text{sup}}^{\text{lat}}(d) = \begin{cases} 1, & 1 \leq d < d', \\ [(1 - \sqrt{3})(d-2) + \sqrt{3}]/2, & d' \leq d < 2, \\ (\sqrt{3}/2 - 1)(d-1) + 1, & 2 \leq d \leq 3, \end{cases} \quad (36b)$$

where $d' := 3 - 1/(\sqrt{3} - 1) \simeq 1.63$. See Fig. 5 for an illustration. While it would be natural to choose f^{lat} so that the dimensionally continued lattice had effective cubic symmetry (discussed in Sec. V C), it is not possible

⁵ Note that many of these hyperlattices are actually shifted lattices, mathematically speaking.

to do so. If we consider, for instance, $d = 5/2$, then the \mathbb{Z}^{d-1} hyperlattices have theta series $1 + 3q + O(q^2)$, while the theta series for the $\mathbb{Z}^{d-1} + (1/2)^{d-1}$ hyperlattices is $2^{3/2}q^{3/8}[1 + O(q^2)]$. The irrational prefactor in the second theta series is a clear obstruction to obtaining effective cubic symmetry: There is no way of obtaining an irrational contribution from the first theta series, since all its coefficients are rational.

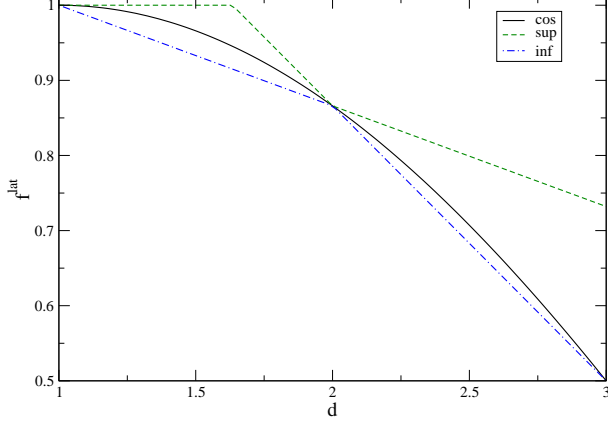


FIG. 5: Plots of f^{lat} [given in Eq. (35)], along with the point-wise sup and inf over all such possibilities [$f_{\text{sup}}^{\text{lat}}$ and $f_{\text{inf}}^{\text{lat}}$, given in Eqs. (36)].

Now, we dimensionally continue the sums over the hyperlattices using the hyperlattice's theta series, which are naturally dimensionally continued. Specifically, the theta series of \mathbb{Z}^d and $\mathbb{Z}^d + (1/2)^d$ are ϑ_3^d and ϑ_2^d , where

$$\vartheta_2(q) := \sum_{k \in \mathbb{Z}} q^{(k+1/2)^2}, \quad \vartheta_3(q) := \sum_{k \in \mathbb{Z}} q^{k^2}, \quad (37a)$$

$$\vartheta_4(q) := \sum_{k \in \mathbb{Z}} (-q)^{k^2}. \quad (37b)$$

See, e.g., Sec. 5 of Chap. 4 of Conway and Sloane [51], but recall the differences in their theta function notation, discussed below Eq. (31). We also introduce ϑ_4 here since it appears in the theta series of the dual lattice.

The theta series of the full lattice is thus

$$\begin{aligned} \bar{\Theta}_\Lambda(z) &= \sum_{k \in \mathbb{Z}} \left\{ q^{[2kf^{\text{lat}}(d)]^2} [\bar{\vartheta}_3(z)]^{d-1} \right. \\ &\quad \left. + q^{[(2k+1)f^{\text{lat}}(d)]^2} [\bar{\vartheta}_2(z)]^{d-1} \right\} \\ &= \bar{\vartheta}_3([2f^{\text{lat}}(d)]^2 z) [\bar{\vartheta}_3(z)]^{d-1} \\ &\quad + \bar{\vartheta}_2([2f^{\text{lat}}(d)]^2 z) [\bar{\vartheta}_2(z)]^{d-1}. \end{aligned} \quad (38)$$

One can check that this reduces to the appropriate expressions for $d \in \{1, 2, 3\}$; the theta series for the 3-dimensional bcc lattice and 2-dimensional hexagonal lattice are given in Eqs. (96) and (60) of Chap. 4 of Conway and Sloane [51]. For $d = 1$, we obtain the theta

series for \mathbb{Z} in a nonstandard form—one can convert it to the standard one given above by using the identity $\bar{\vartheta}_2(4z) + \bar{\vartheta}_3(4z) = \bar{\vartheta}_3(z)$ from Eq. (22) in Chap. 4 of Conway and Sloane.

We use Jacobi's formula (which is already dimensionally continued) to obtain the theta series of the dual lattice, viz., [e.g., Eq. (4) in [50], or Eq. (19) in Chap. 4 of Conway and Sloane [51]]

$$\bar{\Theta}_{\Lambda^*}(z) = \sqrt{\det \Lambda}(i/z)^{d/2} \bar{\Theta}_\Lambda(-1/z). \quad (39)$$

When applying Jacobi's formula, we take the volume of the lattice's Voronoi cell to be dimensionally continued in the obvious way, viz., $\sqrt{\det \Lambda} = f^{\text{lat}}(d)$. [N.B.: This expression neglects the overall scaling of the lattice, which we fix in Eq. (49).] We then obtain, upon use of the theta function identities in Eq. (21) of Chap. 4 in Conway and Sloane,

$$\begin{aligned} \bar{\Theta}_{\Lambda^*}(z) &= \left\{ \bar{\vartheta}_3(z/[2f^{\text{lat}}(d)]^2) [\bar{\vartheta}_3(z)]^{d-1} \right. \\ &\quad \left. + \bar{\vartheta}_4(z/[2f^{\text{lat}}(d)]^2) [\bar{\vartheta}_4(z)]^{d-1} \right\} / 2 \\ &= \frac{1}{2} \sum_{k \in \mathbb{Z}} \left\{ q^{[kf^{\text{lat}}(d)]^2} \left([\bar{\vartheta}_3(z)]^{d-1} + [\bar{\vartheta}_4(z)]^{d-1} \right) \right. \\ &\quad \left. + q^{[(k+1/2)/f^{\text{lat}}(d)]^2} \left([\bar{\vartheta}_3(z)]^{d-1} - [\bar{\vartheta}_4(z)]^{d-1} \right) \right\}. \end{aligned} \quad (40)$$

The second expression tells us that we can treat the dual lattice as a union of hyperlattices separated by a distance of $[2f^{\text{lat}}(d)]^{-1}$, where the even hyperlattices are D_{d-1} and the odd ones are $D_{d-1} + (0^{d-2}1)$ (cf. the schematic of the direct lattice shown in Fig. 4). Here D_d is the d -dimensional root lattice discussed in Sec. 7.1 of Chap. 4 of Conway and Sloane [51], and $D_d + (0^{d-1}1)$ denotes the same lattice shifted by a unit in one coordinate direction. These lattices' theta series are [Eqs. (87) and (89) of Chap. 4 of Conway and Sloane [51]] $(\vartheta_3^d \pm \vartheta_4^d)/2$, with the upper [resp. lower] sign corresponding to D_d [resp. $D_d + (0^{d-1}1)$]. This interpretation is convenient, as it allows us to compute the sums over the dual lattice using the same technology as for the direct lattice.

C. Lattice sums

From the expressions in Eqs. (15)–(20), we see that we need to dimensionally continue sums involving a spherically symmetric function times either x_1^n ($n \in \{0, 2, 4\}$), x_2^2 , or $x_1^2 x_2^2$. In order to do this with our method, we note that we can express x_1^n in terms of $f^{\text{lat}}(d)$ and the index of the hyperlattice (k , in our discussion below), due to our method of dimensionally continuing the lattice. For x_2^2 , we note that the hyperlattices have effective cubic symmetry, so we have

$$\sum_{\vec{x} \in \mathcal{H}_{d-1} \cap S_r} x_2^2 = \frac{n_{\mathcal{H}}(r)r^2}{d-1}, \quad (41)$$

where $\mathcal{H}_{d-1} \cap S_r$ denotes the intersection of a hyperlattice \mathcal{H}_{d-1} (with dimension $d-1$) with a $(d-2)$ -sphere of radius r centered at the origin, and $n_{\mathcal{H}}(r)$ is the number of points in this intersection (obtained from \mathcal{H}_{d-1} 's theta series). Unfortunately, this method is not applicable to x_2^4 (which appears in the Fuchs expression for A_{lat} along with x_1^4), which is why we compute A_{lat} using the more involved method discussed above. However, note that we can compute P_{es} (and thus A_{lat}) and c_{44} two ways—the lattice sums we use do not contain fourth powers of any of the coordinates, so we can also compute them with the index substitution $1 \leftrightarrow 2$. We find that the two choices differ by $\lesssim 10\%$. Since these would be exactly equal if effective cubic symmetry held, this gives an indication that our assumption of such symmetry is valid to about this level.

We now give the explicit expressions for the computation of the requisite lattice sums in a dimensionally continued manner. If we consider summing $G(x_1, x_2)F(\|\vec{x}\|)$ over the d -dimensional lattice Λ_d , where $G(x_1, x_2)$ is either one of x_1^n ($n \in \{0, 2, 4\}$), x_2^2 , or $x_1^2 x_2^2$, then we have to evaluate the following double sum:

$$\sum_{\vec{x} \in \Lambda_d} G(x_1, x_2)F(\|\vec{x}\|) = \sum_{k=0}^{\infty} \sum_{l=0}^{\infty} \left\{ \iota_k N_l^{[3]} \mathcal{A}_G F(\mathcal{R}^{[3]}) + 2N_l^{[2]} \mathcal{B}_G F(\mathcal{R}^{[2]}) \right\}, \quad (42)$$

where

$$\mathcal{A}_{x_1^n} = [2k f^{\text{lat}}(d)]^n, \quad \mathcal{B}_{x_1^n} = [(2k+1) f^{\text{lat}}(d)]^n, \quad (43a)$$

$$\mathcal{A}_{x_2^2} = l/(d-1), \quad \mathcal{B}_{x_2^2} = l/(d-1) + 1/4, \quad (43b)$$

$$\mathcal{R}^{[3]} := \sqrt{[2k f^{\text{lat}}(d)]^2 + l}, \quad (43c)$$

$$\mathcal{R}^{[2]} := \sqrt{[(2k+1) f^{\text{lat}}(d)]^2 + l + (d-1)/4}, \quad (43d)$$

and one obtains the coefficients for the $x_1^2 x_2^2$ case by multiplication (e.g., $\mathcal{A}_{x_1^2 x_2^2} = \mathcal{A}_{x_1^2} \mathcal{A}_{x_2^2}$). [The superscripts [2] and [3] come from the names of the theta functions that give the pertinent hyperlattices' theta series—see Eq. (45).] The l -sum comes from summing over an individual hyperlattice, and the k -sum then sums over all hyperlattices. We have introduced

$$\iota_k := \begin{cases} 1, & k=0, \\ 2, & \text{otherwise,} \end{cases} \quad (44)$$

so we can take k to run only over the positive integers, while the hyperlattice index runs over *all* integers. The structure of the hyperlattices is accounted for by the theta series coefficients $N_l^{[j]}$, defined by

$$\sum_{l=0}^{\infty} N_l^{[3]} q^l := [\vartheta_3(q)]^{d-1}, \quad \sum_{l=0}^{\infty} N_l^{[2]} q^l := \left[\frac{\vartheta_2(q)}{q^{1/4}} \right]^{d-1} \quad (45)$$

[recall that the hyperlattices' theta series are ϑ_2^{d-1} and ϑ_3^{d-1} ; the theta functions are defined in Eq. (37a)]. Similarly, for the dual lattice, we have

$$\sum_{\vec{p} \in \Lambda_d^*} G(p_1, p_2)F(\|\vec{p}\|) = \sum_{k=0}^{\infty} \sum_{l=0}^{\infty} \left\{ \iota_k N_l^+ \mathcal{C}_G F(\mathcal{R}^+) + 2N_l^- \mathcal{D}_G F(\mathcal{R}^-) \right\}, \quad (46)$$

where

$$\mathcal{C}_{p_1^n} = [k/f^{\text{lat}}(d)]^n, \quad \mathcal{D}_{p_1^n} = [(k+1/2)/f^{\text{lat}}(d)]^n, \quad (47a)$$

$$\mathcal{C}_{p_2^2} = 2l/(d-1), \quad \mathcal{D}_{p_2^2} = (2l+1)/(d-1), \quad (47b)$$

$$\mathcal{R}^+ := \sqrt{[k/f^{\text{lat}}(d)]^2 + 2l}, \quad (47c)$$

$$\mathcal{R}^- := \sqrt{[(k+1/2)/f^{\text{lat}}(d)]^2 + 2l + 1}, \quad (47d)$$

(with the same multiplication for the $p_1^2 p_2^2$ case as for the direct lattice), and the theta series coefficients are given by

$$\sum_{l=0}^{\infty} N_l^{\pm} q^l := \{ [\vartheta_3(q)]^{d-1} \pm [\vartheta_4(q)]^{d-1} \} / 2 \quad (48)$$

[recall that the dual hyperlattices' theta series are $\vartheta_3^{d-1} \pm \vartheta_4^{d-1}$].

We can now calculate the elastic constants by combining together these results with our previously derived expressions. For c_{44} , these are given by Eqs. (15) and (16). For A_{lat} and A_{\perp} , one uses the sums given in Eqs. (21) and (25), respectively. We also need to determine the scaling of the lattice for a given energy density. This is given by the cell radius, R , computed in Sec. II C: Equating the volume of a cell with this radius to the volume of the lattice's Voronoi cell [given by $f^{\text{lat}}(d)a^d$] determines the lattice's spacing, a . Explicitly, we have

$$a = \frac{\pi^{1/2}}{[f^{\text{lat}}(d)\Gamma(d/2+1)]^{1/d}} R, \quad (49)$$

using the dimensionally continued expression for the volume of a unit d -ball, viz., $\pi^{d/2}/\Gamma(d/2+1)$. Additionally, we compute Q , the charge of the blob, using the charge density of the rare phase and the (d -dimensional) volume of the blob.

VI. RESULTS AND DISCUSSION

Here we present the shear moduli for the various EOS parameters we consider (given in Table I).

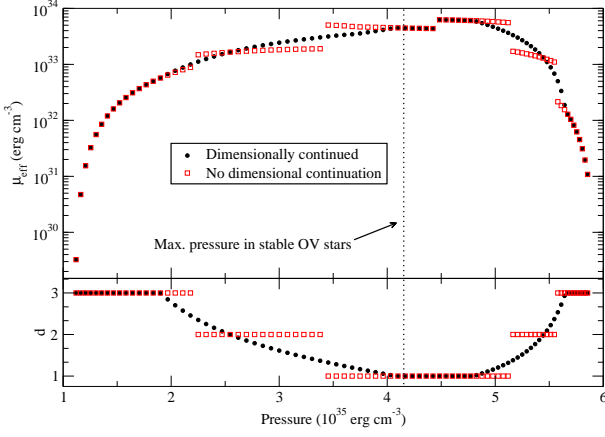


FIG. 6: The effective shear modulus and lattice dimensionality versus pressure for the Hy1 EOS both with and without dimensional continuation. We have also indicated the maximum pressure one obtains in a stable OV star using this EOS.

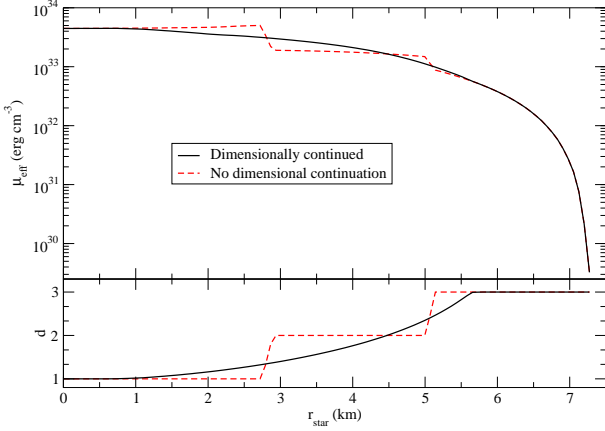


FIG. 7: The effective shear modulus and lattice dimensionality versus OV (Schwarzschild coordinate) radius for the maximum mass stable star (of total radius 12.5 km) with the Hy1 EOS both with and without dimensional continuation.

First, to give an indication of the effects of dimensional continuation, in Fig. 6 we plot the effective shear modulus μ_{eff} [see Eq. (13)] and lattice dimensionality d versus pressure with and without dimensional continuation, for the Hy1 EOS with a surface tension of $\sigma = 80 \text{ MeV fm}^{-2}$ [and the $f_{\text{cos}}^{\text{lat}}$ lattice interpolation function from Eq. (35)]. We have shown all the pasta phases, even though only the first few appear in stable stars, as is indicated in the figure. The jump in the effective shear modulus occurs at the halfway point—i.e., equal amounts of quark and hadronic matter—and is due to the switch on the screening length λ at that point (see the discussion in Sec. IID). Also note that the lattice becomes unstable for a small range of d slightly less than 3—see the discussion below. We additionally show μ_{eff} and d versus the (Schwarzschild coordinate) OV stellar radius r_{star} for the

maximum mass star in Fig. 7.

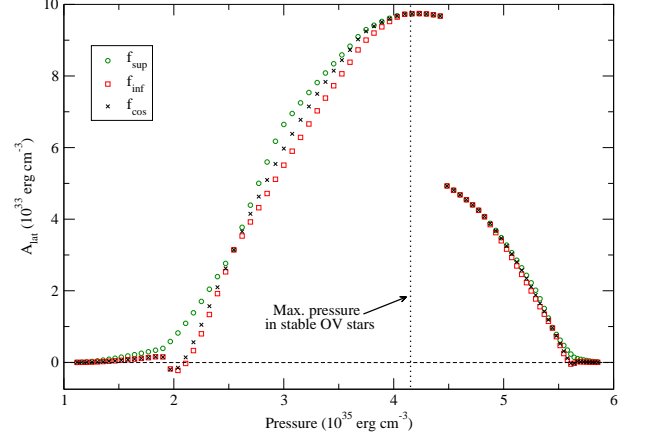


FIG. 8: The (dimensionally continued) A_{lat} versus pressure for the Hy1 EOS and a variety of f^{lat} s. See the text for a discussion of the small unphysical dip below zero.

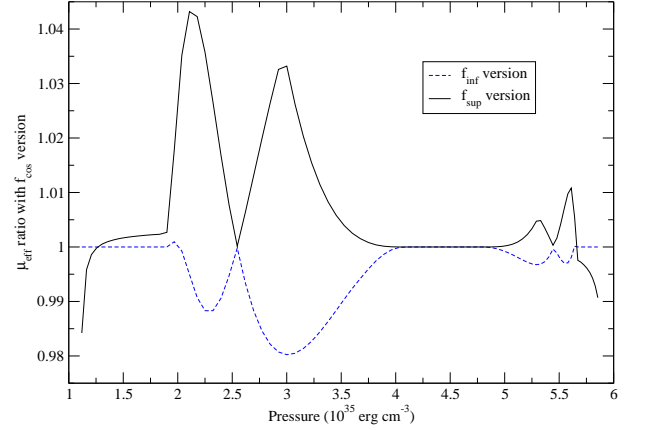


FIG. 9: Ratios of the effective shear modulus computed using $f_{\text{sup}}^{\text{lat}}$ and $f_{\text{inf}}^{\text{lat}}$ to that computed using $f_{\text{cos}}^{\text{lat}}$ [see Eqs. (35) and (36)] plotted versus pressure for the Hy1 EOS and $\sigma = 80 \text{ MeV fm}^{-2}$. Thus the error due to our lack of knowledge of this function is at most about 5% in small regions of the star.

Even if the effective shear modulus is positive, the lattice can still be unstable to shear strains if A_{lat} is negative. This is the case for small regions of the lattice whose effective shear modulus is shown in Fig. 6, specifically, where d is slightly less than 3. However, one only obtains such an instability when one uses $f_{\text{cos}}^{\text{lat}}$, $f_{\text{inf}}^{\text{lat}}$, or something similar for the lattice interpolation function. If one uses $f_{\text{sup}}^{\text{lat}}$, then A_{lat} remains positive. This is illustrated in Fig. 8 for the same Hy1 $\sigma = 80 \text{ MeV fm}^{-2}$ case, using the lattice interpolation function $f_{\text{cos}}^{\text{lat}}$ as well as the sup and inf over all interpolation functions [given in Eqs. (36)]. We do not use $f_{\text{sup}}^{\text{lat}}$ itself in our shear modulus calculations because it does not satisfy the smooth-

ness and convexity criteria, though Fig. 8 indicates that an f^{lat} that was somewhat greater than $f_{\text{COS}}^{\text{lat}}$ for d near 3 would not lead to the instabilities. Regardless, the variations in shear modulus are at most 5% between sup and inf in small regions, as illustrated in Fig. 9, so we tolerate this small inconsistency.

The sign issue does not arise with A_{\perp} , which is made positive by the contributions from changing the cell size [cf. Eq. (25)]. While c_{11} is always negative, $A_{\perp, \text{cell}}$ is enough to make A_{\perp} positive except for $d \simeq 2.99$, where $A_{\perp, Q}$ is also needed in certain cases. There $A_{\perp, Q}$ is positive, although it is negative for $d \lesssim 2$.

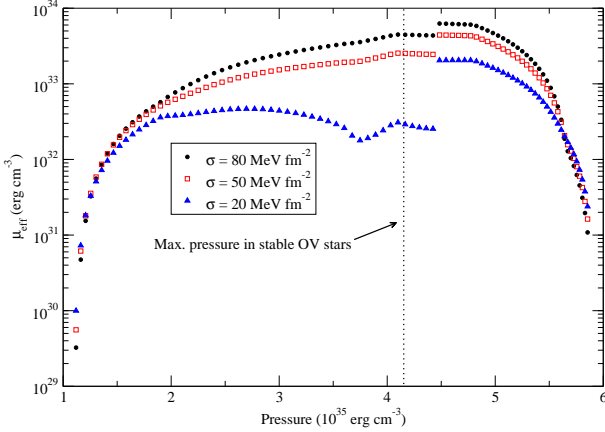


FIG. 10: The (dimensionally continued) effective shear modulus versus pressure for the Hy1 EOS and a variety of surface tensions, σ . The discontinuity, which does not occur in a real star, is largely caused by our simplified treatment of charge screening and serves as an estimate of the error in that treatment. For high or moderate surface tensions, that error is less than a factor 2. For low surface tension the error can be an order of magnitude, but these lattices are nearly unstable in any case, as shown below.

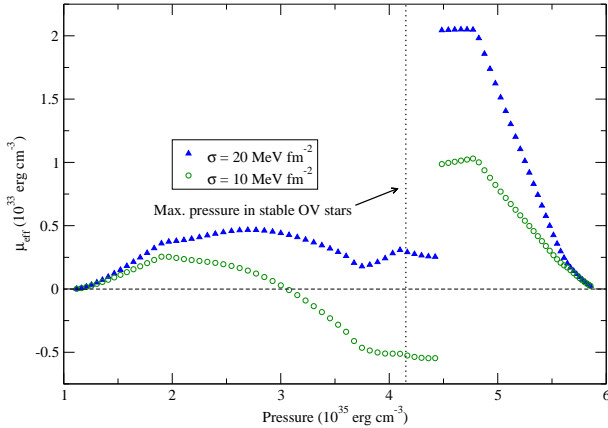


FIG. 11: The (dimensionally continued) effective shear modulus versus pressure for the Hy1 EOS and two choices of σ , showing the negative values for $\sigma = 10 \text{ MeV fm}^{-2}$.

The largest effect of the equation of state parameters on observable quantities involving the shear modulus is the extent of the mixed phase in stable stars. See Weissenborn *et al.* [20] for a survey of the dependence of the mixed phase’s extent on the bag constant and QCD coupling constant for two hadronic EOS parameter sets.

The largest effect on the shear modulus itself, however, comes from the surface tension, σ . This is illustrated for the Hy1 EOS in Fig. 10. (The magnitude of the reduction of the shear modulus with decreasing surface tension also holds for the other EOSs we consider.) Note that the shear modulus is greater for smaller surface tensions for d close to 3. Additionally, σ has a direct, and quite substantial, effect on the lattice’s stability: If σ is too small, then the lattice will become unstable to shears (indicated by A_{\perp} becoming negative) as the dimensionality decreases, as illustrated for the Hy1 EOS and two small values of σ in Fig. 11. A surface tension that is much higher than the range we consider makes any lattice too energetically expensive to form.

To illustrate the relatively small effect of the other EOS parameters on the effective shear modulus for a fixed surface tension, we plot μ_{eff} versus the quark volume fraction χ for a representative sample of the EOSs from Table I with $\sigma = 80 \text{ MeV fm}^{-2}$ in Fig. 12. The different flavors of Hy1 EOS—i.e., Hy1, Hy1 μ , Hy1 σ , Hy1 $\mu\sigma$ —all have quite similar shear moduli for a fixed surface tension. The inclusion of the surface tension contribution to the pressure balance causes the largest difference of any of these other EOS parameters, but even this difference is considerably smaller than the differences between the EOSs shown in the figure, and is negligible where the shear modulus is largest. We have thus not shown the traces for those EOSs, to avoid a cluttered figure.

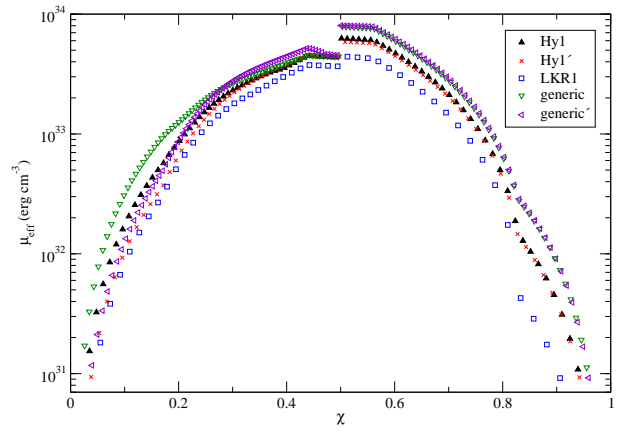


FIG. 12: The (dimensionally continued) effective shear modulus versus χ for a representative selection of the EOSs from Table I and $\sigma = 80 \text{ MeV fm}^{-2}$. We have left off a few points at either extreme of χ with low shear moduli to better show the differences between the different predictions where the shear moduli are the highest and most astrophysically relevant. There the uncertainty in shear modulus due to factors other than surface tension is at most about a factor of 2.

It is interesting to compare these shear modulus values to those for the lattice of nuclei in the neutron star crust as well as those for crystalline color superconducting (CSC) quark matter: The crustal shear modulus ranges from $\sim 6 \times 10^{27}$ to $\sim 2 \times 10^{30}$ erg cm $^{-3}$ (see, e.g., Fig. 2 in [89]), while the shear modulus of CSC quark matter computed by Mannarelli, Rajagopal, and Sharma (MRS) [7] could be as large as $\sim 4 \times 10^{34}$ erg cm $^{-3}$; the lower bound they give is $\sim 8 \times 10^{32}$ erg cm $^{-3}$. The hadron–quark mixed phase shear moduli we have computed range from $\sim 10^{30}$ erg cm $^{-3}$ for small blobs to $\sim 8 \times 10^{33}$ erg cm $^{-3}$ for hadronic slabs (with a surface tension of $\sigma = 80$ MeV fm $^{-2}$). Thus the mixed-phase shear modulus is at least comparable to the largest shear modulus in the crust and can be three orders of magnitude higher than it, and the largest mixed-phase shear modulus is an order of magnitude less than the largest CSC quark matter shear modulus, roughly the geometric mean of the range given by MRS. (Note, however, that the maximum mixed-phase shear modulus for a given set of EOS parameters is not necessarily realized in a stable star.)

VII. CONCLUSIONS

We have made a more careful calculation of the shear modulus of the hadron–quark mixed phase than has previously been attempted [12, 25, 26]. In particular, we have computed all the lattice’s (anisotropic) shear elastic constants, before averaging to obtain an isotropic effective shear modulus for a polycrystal. We have also dealt with the lattice’s changing dimension in both the electrostatic potential and the geometrical effects on the elastic constants. Perhaps most importantly, we have included the contributions to the elastic constants from changing the size of the blobs for $d < 3$. These act to stabilize the lattice for lower dimensions (leading to significant contributions to the shear modulus from these portions of the lattice), though only for sufficiently large surface tensions. We have found that for our choices of parameters, most of the lower-dimensional portions of the lattice are unstable to shear perturbations if the surface tension is less than 10–20 MeV fm $^{-2}$. (As discussed in [24, 71], the mixed phase is not favored if the surface tension is too large. However, as we mention in Sec. II C, and will explore in depth in [36], these are local energy considerations, while the mixed phase may still be favored by global energy considerations.)

These calculations depend upon a wide variety of poorly constrained parameters. While we found that the shear modulus of the mixed phase itself depends most sensitively on the surface tension, astrophysical effects depend on the amount of mixed phase present in a given star, which is primarily determined by the standard hybrid EOS parameters. We will see this in more detail when we use the shear moduli calculated here to compute the maximum elastic quadrupolar deformations of

these hybrid star models in a companion paper [36].

The obvious place where the shear modulus calculation could be improved significantly is the treatment of charge screening: We know from the calculations of Endo *et al.* [40, 90] that including (nonlinear) charge screening in the computation of the cell energy leads to significant differences in the lattice properties at a given density. Here one would like to at least use the Thomas–Fermi approximation, if one did not perform a nonlinear calculation as in [40, 90]. The shear modulus will be affected both by the change in cell size and spacing, as well as through the cell energy’s direct contribution to one of the elastic constants for lower dimensions. Since this contribution is necessary to stabilize the lattice for those dimensions, it would be interesting to see whether our discovery that the lattice is only stable for sufficiently large surface tensions still holds with charge screening. For instance, there will be, in effect, Fermi contributions to the cell energy in a proper treatment.

One might also want to investigate the effects of using different descriptions of the hadronic and quark matter. For instance, for the quark matter, one could use the higher-order perturbative calculations of Kurkela, Romatschke, and Vuorinen [66] or the Nambu–Jona-Lasinio treatment (e.g., [22, 91]), while Dirac–Brueckner–Hartree–Fock (e.g., [91]) would be a possibility for the hadronic matter. One might also investigate the potential effects of color superconductivity (see [6] for a review): The inclusion of CSC quark matter would, of course, increase the shear modulus (see Mannarelli, Rajagopal, and Sharma [7] for a calculation of the shear modulus of bulk CSC quark matter). However, if one does not have a crystalline phase, color superconductivity would primarily affect these shear modulus calculations through the EOS, where Alford *et al.* [65] find that including color superconductivity reduces the transition density to quark matter, but does not appreciably change the maximum mass. While one would also expect color superconductivity to affect the energy of the quark blobs, and thus the contributions to the shear modulus from changing the blob size, we have not even included quark interaction contributions to the blob energy in the present calculation, only considering the electrostatic contributions. Other possibilities for extending the calculation overall would be including more exotica (hyperons, for instance, as in, e.g., [21, 22, 59]), and, in particular, magnetic fields [cf. the discussion in Baiko [49] and below our Eq. (12)].

One could also apply our methods of calculating the shear modulus of the pasta phases to the nuclear pasta appearing in the crust. Such a calculation would be particularly interesting given recent studies of the observational effects of the crustal pasta which used very rough models for its shear modulus [92, 93]. Our methods could also be adapted to calculate the shear moduli of meson condensates more carefully than the existing order of magnitude estimates (Ref. [26] and references therein).

The shear moduli here can be several hundred times larger than those first estimated [12]. Naïvely, one might

expect the maximum quadrupole to go up by a similar factor, but this is complicated by issues of where the various lattices occur in the star. We will present an exploration of that and other issues with the maximum quadrupole elsewhere [36].

Acknowledgments

We are grateful to M. Alford and C. Horowitz for helpful discussions. This work was supported by NSF grants PHY-0555628 and PHY-0855589, the Eberly research funds of Penn State, and the DFG SFB/Transregio 7.

Appendix: Checks of lattice sums

We have checked that our code can reproduce all the relevant results for elastic constants presented in the literature, and detail these checks here: For a three-dimensional unscreened bcc lattice, we have checked that we can reproduce the results of Fuchs [48] (for c_{44} and A_{lat}) and Ho [94] (for c_{11}), and also that we are in agreement with the very recent and much more precise calculation of all three elastic constants (to 8 significant digits) by Baiko [49]. For a three-dimensional bcc lattice with screening, we have checked against the results from Horowitz and Hughto [95]. We have also checked that the surprisingly simple results we obtain in the unscreened two-dimensional hexagonal case agree with those obtained analytically using zeta function regularization.

Numerical agreement is good. We reproduce the Fuchs results to better than 0.25% for A_{lat} and 0.015% for c_{44} . Moreover, we agree with Baiko's results to all five significant figures to which we have calculated them (using a screening length of $10^{10}a$). Baiko claims agreement with Fuchs and does not comment on the discrepancy, which we conjecture is due to modern computational technology allowing for the summation of more terms. We agree with Ho's result to the four significant figures to which he gives it. Horowitz and Hughto computed A_{lat} (twice their b_{11}) for a screening length of $\lambda = 0.863a$. We agree to better than 1% for A_{lat} and 0.011% for c_{44} . The discrepancy for c_{44} could be due to rounding. The discrepancy for A_{lat} is compatible with Horowitz and Hughto's caveat about a 1% error in that part of their calculation due to using a brute force summation rather than the Ewald method.⁶

For the two-dimensional unscreened hexagonal lattice, we obtain what appear numerically to be simple fractions

for the elastic constants (when expressed in Fuchs-type units of Q^2). Explicitly, we have $A_{\text{lat}} = 1/2$, $c_{11} = -1/4$, and $c_{44} = 1/4$.

We can show that these elastic constants indeed take the expected, extremely simple forms by calculating them analytically using analytic continuation of an Epstein zeta function, as discussed in, e.g., [96, 97]. (A calculation of these elastic constants for a 2-dimensional Coulomb lattice does not appear to exist in the literature.) We first note that the 2-dimensional Coulomb potential is $-2Q \log r$. Thus the sums that give the elastic constants will all have the formal (and divergent) form

$$\sum'_{\vec{x} \in \Lambda_{\text{hex}}} \alpha, \quad (\text{A.1})$$

where α is some constant and Λ_{hex} is the hexagonal lattice. To see this explicitly for c_{11} , we have (writing it in Fuchs-type units)

$$c_{11}^{\text{hex}} = - \sum'_{\vec{x} \in \Lambda_{\text{hex}}} \left(\frac{x_1^2}{\|\vec{x}\|^2} - 2 \frac{x_1^4}{\|\vec{x}\|^4} \right) = \sum'_{\vec{x} \in \Lambda_{\text{hex}}} \frac{1}{4}, \quad (\text{A.2})$$

where we have used the substitutions $x_1^2 \rightarrow \|\vec{x}\|^2/2$ and $x_1^4 \rightarrow (3/8)\|\vec{x}\|^4$ (valid when summing over a hexagonal lattice). (One can obtain these substitutions by direct calculation, for which it is convenient to write the lattice points as elements of \mathbb{C} , so one can multiply a given point by sixth roots of unity to obtain all the other lattice points the same distance from the origin.)

Of course, this sum diverges, but, as indicated in Sec IV, we expect to obtain a regularized version from our Ewald sum procedure. Indeed, it seems reasonable (possibly even likely) that we should obtain the same result using Ewald sums as one obtains using zeta function regularization, since both methods rely at their root on the Jacobi imaginary transformation of theta functions: See, for instance, the discussion in [50], which obtains the Poisson summation formula used in the Ewald method from the Jacobi transformation, and the discussion in Appendix B of [96], which analytically continues the Epstein zeta function using the Jacobi imaginary transformation of theta functions (referred to by its alternate name of the modular property of the theta function).

We thus begin by defining the Epstein zeta function ζ_{Λ} associated with an arbitrary lattice Λ . This is given [cf. the version for \mathbb{Z}^d in Eq. (B1) of [96] and the more general version in Eq. (2.5) of [97]] by

$$\zeta_{\Lambda}(s) := \sum'_{\vec{x} \in \Lambda} \frac{1}{\|\vec{x}\|^{2s}} \quad (\text{A.3})$$

for $\text{Re } s > d/2$ (where d is the dimension of Λ), and analytically continued to $s \in \mathbb{C}$ (except for isolated poles) by Riemann's integral-splitting procedure and the Jacobi imaginary transformation, as in [96, 97]. We have $\zeta_{\Lambda}(0) = -1$ for any lattice [of positive dimension—cf. the third property given in Appendix B of [96] and Eq. (2.13)

⁶ N.B.: Horowitz and Hughto's expression for b_{11} in terms of c_{11} and c_{12} in their Eq. (13) is missing a factor of 1/2, which can be seen to be present by starting from Eq. (7) in [83] and noting that $c_{31} = c_{12}$ for a cubic lattice.

in [97]], so we obtain $c_{11} = -1/4$, in Fuchs-type units, as advertised above. We obtain the values for c_{44} and A given above by the same procedure, except that we also

need to use the additional hexagonal lattice sum substitution $x_1^2 x_2^2 \rightarrow \|\vec{x}\|^4/8$.

-
- [1] J. C. Collins and M. J. Perry, Phys. Rev. Lett. **34**, 1353 (1975).
- [2] N. Itoh, Prog. Theor. Phys. **44**, 291 (1970).
- [3] A. Bodmer, Phys. Rev. D **4**, 1601 (1971).
- [4] E. Witten, Phys. Rev. D **30**, 272 (1984).
- [5] M. G. Alford, K. Rajagopal, and F. Wilczek, Nucl. Phys. **B537**, 443 (1999).
- [6] M. G. Alford, A. Schmitt, K. Rajagopal, and T. Schafer, Rev. Mod. Phys. **80**, 1455 (2008).
- [7] M. Mannarelli, K. Rajagopal, and R. Sharma, Phys. Rev. D **76**, 074026 (2007).
- [8] B. Abbott *et al.* (LIGO Scientific Collaboration), Phys. Rev. D **76**, 062003 (2007).
- [9] B. Abbott *et al.* (LIGO Scientific Collaboration), Astrophys. J. Lett. **683**, L45 (2008), **706**, L203(E) (2009).
- [10] J. Abadie *et al.* (LIGO Scientific Collaboration), Astrophys. J. **722**, 1504 (2010).
- [11] J. Abadie *et al.* (LIGO Scientific Collaboration and Virgo Collaboration), Astrophys. J. Lett. **734**, L35 (2011).
- [12] B. J. Owen, Phys. Rev. Lett. **95**, 211101 (2005).
- [13] N. K. Glendenning, Nucl. Phys. B (Proc. Suppl.) **24**, 110 (1991).
- [14] N. K. Glendenning, Phys. Rev. D **46**, 1274 (1992).
- [15] N. K. Glendenning, Phys. Rep. **342**, 393 (2001).
- [16] N. K. Glendenning, *Compact Stars: Nuclear Physics, Particle Physics, and General Relativity* (Springer-Verlag, New York, 2000), 2nd ed.
- [17] P. B. Demorest, T. Pennucci, S. M. Ransom, M. S. E. Roberts, and J. W. T. Hessels, Nature (London) **467**, 1081 (2010).
- [18] F. Özel, D. Psaltis, S. Ransom, P. Demorest, and M. Alford, Astrophys. J. Lett. **724**, L199 (2010).
- [19] T. Klähn, D. Blaschke, and F. Weber, arXiv:1101.6061 [nucl-th] [Phys. Part. Nucl. Lett. (to be published)].
- [20] S. Weissenborn, I. Sagert, G. Pagliara, M. Hempel, and J. Schaffner-Bielich, Astrophys. J. Lett. **740**, L14 (2011).
- [21] H. Chen, M. Baldo, G. F. Burgio, and H.-J. Schulze, Phys. Rev. D **84**, 105023 (2011).
- [22] L. Bonanno and A. Sedrakian, Astron. Astrophys. **539**, A16 (2012).
- [23] D. G. Ravenhall, C. J. Pethick, and J. R. Wilson, Phys. Rev. Lett. **50**, 2066 (1983).
- [24] H. Heiselberg, C. J. Pethick, and E. F. Staubo, Phys. Rev. Lett. **70**, 1355 (1993).
- [25] M. Nayyar, Ph.D. thesis, The Pennsylvania State University (2007).
- [26] P. Haensel, A. Y. Potekhin, and D. G. Yakovlev, *Neutron Stars 1: Equation of State and Structure* (Springer, New York, 2007).
- [27] V. R. Pandharipande, D. Pines, and R. A. Smith, Astrophys. J. **208**, 550 (1976).
- [28] D. Pines, J. Shaham, and M. Ruderman, Nature—Phys. Sci. **237**, 83 (1972).
- [29] B. Abbott *et al.* (LIGO Scientific Collaboration), Phys. Rev. Lett. **101**, 211102 (2008).
- [30] B. P. Abbott *et al.* (LIGO Scientific Collaboration), Astrophys. J. Lett. **701**, L68 (2009).
- [31] B. J. Owen, Classical Quantum Gravity **26**, 204014 (2009).
- [32] M. Pitkin, Mon. Not. R. Astron. Soc. **415**, 1849 (2011).
- [33] B. P. Abbott *et al.* (LIGO Scientific Collaboration and Virgo Collaboration), Astrophys. J. **713**, 671 (2010).
- [34] C. J. Horowitz and K. Kadau, Phys. Rev. Lett. **102**, 191102 (2009).
- [35] A. Corsi and B. J. Owen, Phys. Rev. D **83**, 104014 (2011).
- [36] N. K. Johnson-McDaniel and B. J. Owen, in preparation.
- [37] T. Norsen and S. Reddy, Phys. Rev. C **63**, 065804 (2001).
- [38] D. N. Voskresensky, M. Yasuhira, and T. Tatsumi, Phys. Lett. B **541**, 93 (2002).
- [39] D. N. Voskresensky, M. Yasuhira, and T. Tatsumi, Nucl. Phys. A **723**, 291 (2003).
- [40] T. Endo, Phys. Rev. C **83**, 068801 (2011).
- [41] C. J. Pethick and A. Y. Potekhin, Phys. Lett. B **427**, 7 (1998).
- [42] H. Sonoda, G. Watanabe, K. Sato, K. Yasuoka, and T. Ebisuzaki, Phys. Rev. C **77**, 035806 (2008), **81**, 049902(E) (2010).
- [43] G. Watanabe, H. Sonoda, T. Maruyama, K. Sato, K. Yasuoka, and T. Ebisuzaki, Phys. Rev. Lett. **103**, 121101 (2009).
- [44] C. J. Horowitz, M. A. Pérez-García, D. K. Berry, and J. Piekarewicz, Phys. Rev. C **72**, 035801 (2005).
- [45] C. J. Horowitz and D. K. Berry, Phys. Rev. C **78**, 035806 (2008).
- [46] P. P. Ewald, Ann. Phys. (Leipzig) **369**, 253 (1921).
- [47] R. E. Johnson and S. Ranganathan, Phys. Rev. E **75**, 056706 (2007).
- [48] K. Fuchs, Proc. R. Soc. A **153**, 622 (1936).
- [49] D. A. Baiko, Mon. Not. R. Astron. Soc. **416**, 22 (2011).
- [50] N. K. Johnson-McDaniel, J. Fourier Anal. Appl. **18**, 367 (2012).
- [51] J. H. Conway and N. J. A. Sloane, *Sphere Packings, Lattices and Groups* (Springer-Verlag, New York, 1999), 3rd ed.
- [52] G. Baym, C. Pethick, and P. Sutherland, Astrophys. J. **170**, 299 (1971).
- [53] J. W. Negele and D. Vautherin, Nucl. Phys. A **207**, 298 (1973).
- [54] J. M. Lattimer and M. Prakash, Astrophys. J. **550**, 426 (2001).
- [55] A. Kurkela, P. Romatschke, A. Vuorinen, and B. Wu, arXiv:1006.4062 [astro-ph.HE].
- [56] <http://theory.physics.helsinki.fi/~aekurkel/neutron/>.
- [57] G. A. Lalazissis, J. König, and P. Ring, Phys. Rev. C **55**, 540 (1997).
- [58] B. D. Lackey, M. Nayyar, and B. J. Owen, Phys. Rev. D **73**, 024021 (2006).
- [59] T. Maruyama, S. Chiba, H.-J. Schulze, and T. Tatsumi, Phys. Rev. D **76**, 123015 (2007).
- [60] J. Piekarewicz, J. Phys. G **37**, 064038 (2010).
- [61] B.-A. Li *et al.*, J. Phys. Conf. Ser. **312**, 042006 (2011).
- [62] A. W. Steiner, M. Prakash, J. M. Lattimer, and P. J.

- Ellis, Phys. Rep. **411**, 325 (2005).
- [63] A. Chodos, R. L. Jaffe, K. Johnson, C. B. Thorn, and V. F. Weisskopf, Phys. Rev. D **9**, 3471 (1974).
- [64] E. Farhi and R. L. Jaffe, Phys. Rev. D **30**, 2379 (1984).
- [65] M. Alford, M. Braby, M. Paris, and S. Reddy, Astrophys. J. **629**, 969 (2005).
- [66] A. Kurkela, P. Romatschke, and A. Vuorinen, Phys. Rev. D **81**, 105021 (2010).
- [67] M. B. Christiansen and N. K. Glendenning, Phys. Rev. C **56**, 2858 (1997).
- [68] A. C. Mattingly and P. M. Stevenson, Phys. Rev. D **49**, 437 (1994).
- [69] G. Ganbold, Phys. Rev. D **81**, 094008 (2010).
- [70] K. Nakamura *et al.* (Particle Data Group), J. Phys. G **37**, 075021 (2010).
- [71] M. Alford, K. Rajagopal, S. Reddy, and F. Wilczek, Phys. Rev. D **64**, 074017 (2001).
- [72] M. B. Christiansen and N. K. Glendenning, astro-ph/0008207.
- [73] L. Lindblom, Astrophys. J. **398**, 569 (1992).
- [74] B. Paladini and J. C. Sexton, Phys. Lett. B **448**, 76 (1999).
- [75] D. C. Wallace, Phys. Rev. **162**, 776 (1967).
- [76] N. Chamel and P. Haensel, Living Rev. Relativity **11**, 10 (2008), <http://www.livingreviews.org/lrr-2008-10>.
- [77] T. Strohmayer, H. M. van Horn, S. Ogata, H. Iyetomi, and S. Ichimaru, Astrophys. J. **375**, 679 (1991).
- [78] W. Voigt, *Lehrbuch der Kristallphysik* (Teubner, Leipzig, 1928).
- [79] R. Hill, Proc. Phys. Soc. A **65**, 349 (1952).
- [80] Z. Hashin and S. Shtrikman, J. Mech. Phys. Solids **10**, 343 (1962).
- [81] J. P. Watt, G. F. Davies, and R. J. O'Connell, Rev. Geophys. Space Phys. **14**, 541 (1976).
- [82] J. P. Watt, J. Appl. Phys. **50**, 6290 (1979).
- [83] S. Ogata and S. Ichimaru, Phys. Rev. A **42**, 4867 (1990).
- [84] J. Braithwaite and H. C. Spruit, Nature (London) **431**, 819 (2004).
- [85] J. J. Zach, Phys. Rev. D **65**, 123002 (2002).
- [86] B. R. A. Nijboer and F. W. de Wette, Physica (Utrecht) **23**, 309 (1957).
- [87] C. M. Fortuin, Physica (Utrecht) **86A**, 574 (1977).
- [88] E. M. Stein and G. Weiss, *Introduction to Fourier Analysis on Euclidean Spaces* (Princeton University Press, Princeton, 1971).
- [89] B. Haskell, D. I. Jones, and N. Andersson, Mon. Not. R. Astron. Soc. **373**, 1423 (2006).
- [90] T. Endo, T. Maruyama, S. Chiba, and T. Tatsumi, Prog. Theor. Phys. **115**, 337 (2006).
- [91] D. B. Blaschke, D. Gómez Dumm, A. G. Grunfeld, T. Klähn, and N. N. Scoccola, Phys. Rev. C **75**, 065804 (2007).
- [92] H. Sotani, Mon. Not. R. Astron. Soc. Lett. **417**, L70 (2011).
- [93] M. Gearheart, W. G. Newton, J. Hooker, and B.-A. Li, Mon. Not. R. Astron. Soc. **418**, 2343 (2011).
- [94] P. S. Ho, Phys. Rev. **169**, 523 (1968).
- [95] C. J. Horowitz and J. Hughto, arXiv:0812.2650 [astro-ph].
- [96] R. Contino and A. Gambassi, J. Math. Phys. **44**, 570 (2003).
- [97] M. L. Glasser and I. J. Zucker, in *Theoretical Chemistry: Advances and Perspectives*, edited by H. Eyring and D. Henderson (Academic Press, New York, 1980), vol. 5, pp. 67–139.